

Department of Physics and Astronomy
University of Heidelberg

Master thesis
in Physics
submitted by
Marko Turkalj Orešković
born in Zagreb
2014

Development of a cryogenic vacuum valve and an electromechanical switch for ALPHATRAP

This Master thesis has been carried out by Marko Turkalj Orešković
at the
Max Planck Institute for Nuclear Physics Heidelberg
under the supervision of
Prof.Dr. Klaus Blaum and Dr. Sven Sturm

Entwicklung eines kryogenen Vakuumventil und eines elektromechanischen Schalters für ALPHATRAP:

Ein Penningfallenexperiment zur Bestimmung des g -Faktors des gebundenen Elektrons in schweren, hochgeladenen Ionen, ALPHATRAP, ist im Aufbau am Max-Planck-Institut für Kernphysik in Heidelberg MPIK. Als Teil dieses Experiments wurde eine Vakuumventil und ein elektromechanischer Schalter konstruiert und getestet. ALPHATRAP wird über ein Raumtemperatur-Strahlrohr an die Heidelberg Elektronenstrahl-Ionenquelle (EBIT) angeschlossen werden. Da das Einfangen von hochgeladenen Ionen erfordert ein extrem gutes Vakuum, besser als 10^{-15} mbar, muss der Strom des Hintergrundgases von der Raumtemperatur-Strahlrohr deutlich reduziert werden. Daher wurde ein kryogene-Vakuumventil entwickelt, welches ausreichende Speicherzeiten ermöglicht. Das Ventil wird manuell betätigt, und arbeitet bei kryogenen Temperaturen und in starken Magnetfeldern.

Weiterhin, ist für die Detektionselektronik ein kryogener elektromechanischer Schalter entwickelt worden. Der Schalter wird durch ein piezoelektrisches Element angesteuert. Vorteile gegenüber Halbleiterschaltern sind vernachlässigbare Leckströme, für der Schalter in offener Position, und vernachlässigbare dielektrischen Verluste. Der Schalter ist als einpoliger Schalter entworfen und hat einen Restwiderstand von nur 11 m Ω . Die Entwürfe und erste Testergebnisse der Geräte werden vorgestellt.

Development of a cryogenic vacuum valve and an electromechanical switch for ALPHATRAP:

A Penning trap experiment for the determination of the g -factor of the bound electron in heavy highly-charged ions, ALPHATRAP, is under construction at the Max-Planck-Institute in Heidelberg MPIK. As a part of this experiment, a vacuum valve and an electromechanical switch were constructed and tested. ALPHATRAP will be connected to an electron-beam ion trap (EBIT) via a room temperature beam-line. Since trapping of highly-charged ions requires extremely good vacuum, in excess of 10^{-15} mbar, the external flow of the background gas from the room-temperature beam-line has to be reduced significantly. Therefore, a cryogenic vacuum valve was developed, which enables adequate storage times. The valve is manually actuated, and operates at cryogenic temperatures as well as in strong magnetic fields.

Furthermore, for the image-current detection electronics a cryogenic electromechanical switch was developed. The switch is actuated by a piezoelectric element. Advantages compared to semiconductor devices are negligible leakage currents for the switch being in open position and negligible dielectric losses. The switch is designed as a single-pole single-throw switch and has a residual resistance of only 11 m Ω . The designs and test results of the devices are presented.

Contents

1. Overview	1
2. The ALPHATRAP experiment	3
2.1. Scientific goals	3
2.2. Experimental setup	4
2.3. Motivation for the cryogenic vacuum valve	6
2.4. Motivation for the cryogenic electromechanical switch	7
3. Cryogenic vacuum valve	9
3.1. Overview	9
3.2. Theory of gases for vacuum systems	9
3.2.1. Gas properties	9
3.2.2. Gas Flow	11
3.3. Analytical modeling	15
3.4. Mechanical design	19
3.5. Conductance of the cryogenic vacuum valve	21
3.5.1. The slit model	22
3.5.2. The sealing interface model	23
3.6. Test results	26
3.6.1. Measurement setup and procedure	26
3.6.2. Conductance measurement results	28
3.7. Conclusion	30
4. Cryogenic piezoelectric switch	31
4.1. Operating environment and requirements	31
4.2. Piezoelectric bender plates	33
4.3. Displacement and contact resistance	34
4.3.1. Displacement at cryogenic temperatures	34
4.3.2. Contact resistance at 4 K temperature	36
4.4. Design of the piezoelectric cryogenic switch	39
4.5. Switching a high quality factor resonator using a piezoelectric switch	40
4.5.1. Characteristic of the high quality factor resonator	41
4.5.2. Test setup and procedure for the switch-resonator configuration	42
4.5.3. Measurement results	43
4.6. Conclusion	44

Bibliography	45
A. Appendix	47
A.1. Gas flow relations	47
A.2. Photographs	48
Acknowledgments	51

1. Overview

Within this master thesis two devices were constructed and tested with the aim to be used in ALPHATRAP experiment currently under construction at the Max-Planck-Institute in Heidelberg MPIK. The two devices, a cryogenic vacuum valve and a piezoelectric switch, operate independently of each other in the experiment. Therefore, the content of the work that is presented here is divided into two main separate parts for each of the devices. The cryogenic vacuum valve is presented in chapter 3, while the piezoelectric switch is presented in chapter 4. Each of the chapters ends with a conclusion where test results are summarized. Overview of the ALPHATRAP experiment, where the devices will be implemented, is given in the following chapter.

2. The ALPHATRAP experiment

Objective of the ALPHATRAP experiment, currently under construction at the Max-Planck-Institute in Heidelberg MPIK, is the precise measurement of the gyromagnetic factor (g -factor) of a bound electron in highly-charged ions. ALPHATRAP is closely associated to a foregoing g -factor experiment started by G. Werth, currently hosted by K.Blaum and conducted by S.Sturm et al. at the Johannes Gutenberg-University of Mainz [SWB13] and can be considered as an extension to that experiment. This section will discuss the scientific goals of the ALPHATRAP experiment, give a brief overview of the related Mainz g -factor experiment and describe the experimental setup and motivation for this thesis.

2.1. Scientific goals

The intention of the experiment is to measure the g -factor of the electron in highly charged systems, up to hydrogen-like lead Pb^{81+} , with very high precision in order to test the bound-state quantum electrodynamics (BS-QED) under extreme conditions. Extreme conditions here are primarily related to extremely high field strengths of the nucleus to which electron is exposed in these highly-charged systems.

The Standard Model of physics, here specifically QED theory, is able to predict the g -factor of the electron very accurately. Comparing this value with the value obtained by measurements on highly-charged ions allows to test bound-state quantum electrodynamics calculations with very high precision [SWB13]. In a measurement performed recently by S.Sturm et al. on hydrogen-like silicon $^{28}\text{Si}^{13+}$ at the Johannes Gutenberg-University of Mainz, the g -factor was determined with relative accuracy of $\Delta g/g = 4 \times 10^{-11}$, which is the most accurate determination of g -factor in bound electron systems to date [Stu11]. That measurement, together with theoretical predictions, represents currently the most stringent BS-QED test. The Mainz experiment showed, within the error limits, an exact agreement of theoretical predicted and experimentally obtained value of the g -factor that demonstrates strong validity of the BS-QED theory. The ALPHATRAP experiment will extend these measurements to even higher charged systems, which are not accessible by the Mainz experiment, and therefore rigorously test the BS-QED at the strongest field strengths accessible.

An important tool used for the determination of the g -factor is a Penning trap. It is used to confine charged particles by means of combined electrostatic and mag-

netic fields and it is a central part of many experiments related to measurements with charged particles. The electron g -factor can be found from measuring the free cyclotron frequency and the Larmor frequency of the confined hydrogen-like ion. In a system using Penning traps for detection of a charged particle, a stored ion will perform cyclotron motion under the presence of magnetic field. The frequency ν_c of that motion is detected in a precision trap (PT). To determine a Larmor frequency the ion is transported to an analysis trap (AT), which has a purposely created magnetic inhomogeneity necessary to detect spin direction of a bound electron. Spin flips induced by a microwave radiation in PT are detected within the AT from which the Larmor frequency ν_L can be found. From the two experimentally found frequencies the g -factor of the electron can be determined as a ratio of ν_c and ν_L by the following relation

$$g = 2 \cdot \frac{\nu_L}{\nu_c} \frac{q m}{e M} \quad (2.1)$$

where q and M are charge and mass of the ion and m and e are mass and charge of the electron. In the Mainz experiment, the Penning trap system is located in a hermetically sealed copper chamber situated in the liquid helium cryostat. This setup allows to achieve a rest-gas pressure of better than 10^{-16} mbar. Owing to such low pressures, losing the trapped ions, e.g. due to charge exchange in collision with the rest-gas particles, will not cause problems. A storage time of several months has been obtained even for highest produced charge states, which means that it was possible to conduct measurements on the same single ion for months [Stu11] [Her99].

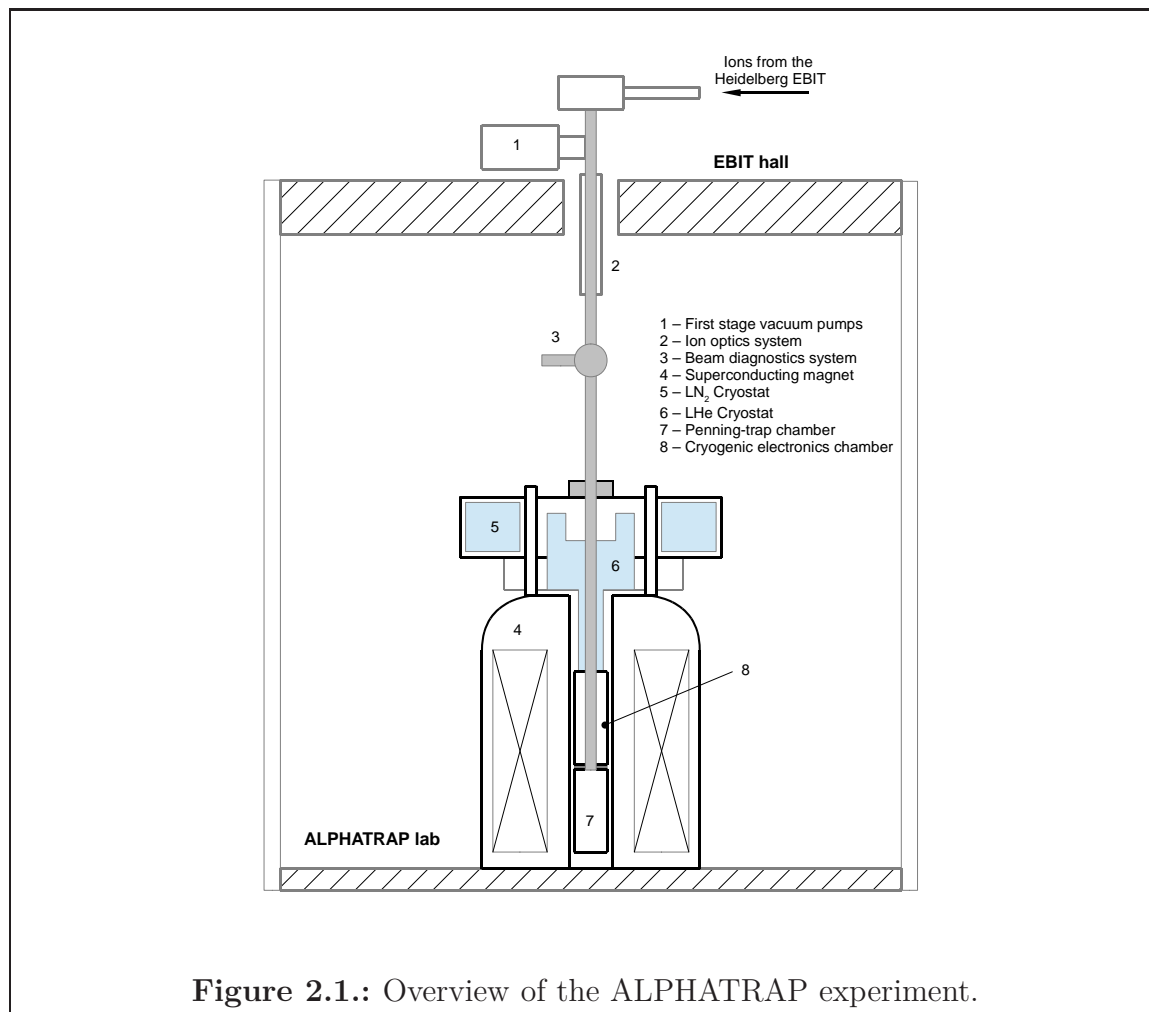
2.2. Experimental setup

The experience gained from the g -factor experiments in the Mainz experiment will also be a valuable foundation for setting up the ALPHATRAP experiment at the MPIK in Heidelberg. ALPHATRAP, also a Penning trap based experiment, is a newly constructed apparatus. Still, the underlying key components (detection electronics, trap design and measurement principle) have similarities to the Mainz experiment. The electron g -factor measurement process is the same as described above, nevertheless, trapping of charged particles up to hydrogen-like lead Pb^{81+} sets demands for completely new design solutions in mechanics as well as in the electronics section of the experiment.

Since the production of heavy highly charged ions is not possible in a small closed system, as the miniature EBIT¹ built in the trap chamber of the Mainz apparatus,

¹Electron Beam Ion Trap : A source of highly charged ions, which are produced by electron beam ionization through confinement in an electromagnetic-magnetic bottle.

the ions for the ALPHATRAP will be produced externally by the “big” Heidelberg EBIT [LUH14]. The externally produced ions are then injected via a room-temperature beam-line into the ALPHATRAP cryogenic trap system. Figure 2.1 shows a drawing of the complete ALPHATRAP setup with EBIT connection. The upper part of the setup consists of ion optics and the diagnostic systems used to center the ion beam trajectory. The ion optics directs the incoming ion beam from the EBIT beam-line down towards the bore of the superconducting magnet where the trap chamber is located. The attached vacuum pumps are used to provide a first-stage vacuum of about 10^{-11} mbar.



The lower part of the setup consists of a superconducting 3.7 T warm-bore magnet, a combined liquid nitrogen/helium cryostat (mounted on top of the magnet housing) and a Penning trap system located in the chamber inside the magnet bore. The cryostat dewar has inserts that fit into the magnet bore, the liquid nitrogen dewar is fixed while the liquid helium dewar can be removed from the magnet bore from above. The trap chamber and ion detection electronics are mounted at the bottom of the liquid helium dewar. Placing the trap and detection electronics as close as

possible to the source of the lowest temperature in the system is essential. This provides better vacuum in the trap chamber by the cryopumping effect and reduces thermal noise in detection electronics, allowing very good signal-to-noise ratio. The liquid nitrogen cryostat provides a temperature shield to the room temperature which reduces a thermal load on the ~ 4 K temperature stage of the liquid helium cryostat. In the ideal case, the magnetic field at the trap location, produced by the superconducting magnet, is homogenous and axially parallel to the cylindrical geometry of the trap.

2.3. Motivation for the cryogenic vacuum valve

Since ALPHATRAP will be connected to the EBIT through a room temperature beam-line, the quality of the vacuum inside the trap chamber becomes a cause of concern. External flow of the rest-gas from the beam-line into the trap chamber volume could result in short storage times of trapped ions. Moreover, since the aim is to trap and do measurements on ions with charge states much higher than in the Mainz experiment, the achieved storage time may be practically unusable. Pinching off the trap chamber is not an option here, since this would result in terminating the passage of ions from the EBIT. The problem could be solved by a device inserted in the beam-line that would function as a vacuum valve. By opening the valve when an ion beam from the EBIT is passing through and closing it when the ion is trapped a significant improvement of the vacuum is aimed for. When closed, the valve should reduce the flow of rest-gas to the extent that it does not affect the measurement process. However, to produce a good reduction of the rest-gas flow the valve should be placed at the lowest temperature in the beam-line. If the valve is placed at a higher temperature, the rest-gas will not be efficiently removed by the cryo-condensation process. For gases having a low condensation temperature (e.g. 4.2 K for helium) the valve is then not an obstacle since they are found beneath the valve. This means that it is essential to place the valve at 4.2 K temperature stage, i.e. close to the liquid helium cryostat dewar where limited space is available. Further requirements that inevitably come with placing the valve at 4.2 K temperature stage are:

- Only non-magnetic materials can be used
- Operation at cryogenic temperatures (4.2 K)
- Suitable for high vacuum environment (UHV/XHV)

The valve has to be non-magnetic in order not to affect the ion trajectories and field homogeneity of the superconducting magnet. Furthermore, it has to be constructed out of material suitable for high vacuum (low out-gassing), taking into account space limitations. Since there was no commercial product that satisfactorily meets the above listed requirements the valve was custom designed, built and tested in the course of this thesis.

2.4. Motivation for the cryogenic electromechanical switch

Constructing a new experimental setup gives the opportunity to make major improvements in the ion detection system, which is a subject of the second part of this (chapter 4). During the measurement process, in certain cases, it is desirable to switch off some of the electronic components of the detection system. Typical solid-state devices used for that purpose (e.g. transistors, diodes) have significant drawbacks, such as leakage currents, RF dielectric losses in the material of the device and non-zero on resistance. The dielectric losses reduce the quality factor of the resonators while the leakage currents and non-zero resistance introduce noise into the detection electronics. These factors limit the precision of the ion detection system. Using a electromechanical switch could have advantages over solid state devices. Since the contact is then mechanically realized, the leakage currents would be negligible, resulting in a lower noise level. Designing a switch in a suitable way can also minimize RF losses, which means less effect on the quality factor of the resonator. Considering that the detection electronics is located just beneath the liquid helium dewar, the switch must operate in the same environment as mentioned for the vacuum valve. This poses a challenge for the construction of the switch, where the primary question is how to actuate the switch. For this purpose it was decided to use a piezoelectric bender plates, since these are suitable for operation in our environment. Within this thesis, a electromechanical switch actuated by a piezoelectric bender plate was constructed, tested and preliminary results are presented.

3. Cryogenic vacuum valve

3.1. Overview

This chapter will first discuss theoretical fundamentals the of vacuum physics and technology. Analytical models concerning the ion storage times and the valve efficiency are given in the subsequent section. Thereafter, mechanical design and conductance models of the valve is presented, which is followed by the test results and conclusive discussion.

3.2. Theory of gases for vacuum systems

This section will introduce some of the elementary concepts in the theory of gases needed for the discussion of vacuum physics. The focus is on the gas flow at low pressures in the molecular flow regime. The description of the gas properties is based on the kinetic theory of gases. Concepts as throughput, pumping speed and conductance, used often in vacuum systems calculations, are introduced. Characterization of the vacuum system often requires a calculation or estimation of the conductance, which has to be found from the conductance of the individual components of the vacuum system. Hence, conductance relations for some typical geometries are given, as well as the relations for calculating the conductance from the combination of the components. The section is based on the material found in [CC05, Jou08, O'H05, Rot12].

3.2.1. Gas properties

Macroscopic gas properties, such as pressure, volume and temperature, can be described within the kinetic theory of gases. It assumes that the individual particles behave like a small hard spheres and that their collisions are perfectly elastic. The kinetic theory allows to describe the ideal gas by the relation know as the ideal gas law

$$pV = Nk_B T, \tag{3.1}$$

where p , V and T are pressure, volume and temperature state variables respectively, N is the number of particles and k_B is the Boltzmann constant. In the real gases, the potential energy between particles results in the interaction forces. This energy

can be approximately deduced from the Lennard-Jones potential [Jou08], which is a function of the distance between the particles. It can explain the deviations from the ideal gas law that occurs to all gases if the pressure is increased or the temperature lowered.

- Deviations at higher pressures

By increasing the pressure, the average distance between the particles decreases and the attraction becomes significant. This results in a pressure that is less than predicted by the ideal gas law. If the pressure is increased even further, eventually the repulsion between the particles becomes dominant, which results in a pressure higher than predicted by the ideal gas law. Therefore, at higher pressures, when a gas particles are close to each other, most of the energy of the real gases will be contained in the potential energy, while the ideal gas considers only the kinetic energy.

- Deviations at lower temperatures

At low temperatures, as the energy of the gas particles decreases, the attractive forces caused by the potential become significant and collision are not any more perfectly elastic. By lowering the temperature further, the colliding gas particles begin to stick to one another and the gas can start to condense.

The pressure or the temperature at which these deviations become significant depends on the type of gas particle. However, at very low pressures, the inelastic effect in the particle collision will lose its relevance. Furthermore, the helium gas, often considered here, consist of small and inert particles with very low attractive potential, which makes it behave very much like the ideal gas. Therefore, although the kinetic theory has limitations, in the following discussion it will be assumed that the ideal gas law holds.

The velocity distribution of the particles in an ideal gas is given by the Maxwell-Boltzmann velocity distribution function, from which the average velocity v_{av} of the gas particle can be calculated [O'H05]. The average velocity of a gas particle at temperature T is given as

$$v_{av} = \sqrt{\frac{8 k_B T}{m}} = \sqrt{\frac{8 R T}{M}}, \quad (3.2)$$

where T is the temperature, m the mass of the gas particle and M (in kg/mole units) is the molar mass of the gas particle and R is the ideal gas constant. Table 3.1 lists average velocity at room and cryogenic temperatures for helium and hydrogen calculated from Equation 3.2.

Gas/T	Average velocity v_{av} (m/s)	
	295 K	77 K
H ₂	1767	903
He	1250	639

Table 3.1.: Average velocity for hydrogen and helium at room and cryogenic temperatures.

The average distance l that a gas particle travels between two successive collisions with the other gas particles is referred to as the mean free path. It is expressed by the following relation

$$l = \frac{1}{\sqrt{2} \pi d^2 n} = \frac{k_B T}{\sqrt{2} \pi d^2 p}, \quad (3.3)$$

where d is the particle diameter, n is the particle number density (particles per unit volume), T is the temperature and p the pressure of the gas. By moving the pressure p to the left hand side of Equation 3.3 the product of the mean free path and the pressure is given by

$$lp = \frac{k_B T}{\sqrt{2} \pi d^2} = 3.1 \times 10^{-24} \frac{T}{d^2}. \quad (3.4)$$

To estimate the mean free path of the helium gas particles, the approximate value for the helium atomic diameter of 2.6×10^{-10} m found in [Rot12] can be used. It follows that the mean free path at pressure of 10^{-3} mbar and temperatures of 295 K and 77 K is about 14 cm and 3 cm respectively.

When a type of gas flow through components in a vacuum system needs to be characterized, the particles mean free path is an important information. For example, in a high vacuum systems, a gas particles will have a large mean free path and are colliding more frequently with the chamber walls than with the other gas particles. In that case the description of the gas flow is based on the theory of statistical mechanics. At higher pressures when the mean free path is smaller, gas can be treated as continuous medium the gas flow description is within the theory of continuum mechanics.

3.2.2. Gas Flow

Knowledge of the pressure and the geometry of a component in a vacuum system is a prerequisite to know the nature of the gas flow, below listed are the pressure ranges typically encountered in a vacuum systems.

- Medium vacuum 1 - 10^{-3} mbar
- High Vacuum 10^{-3} - 10^{-7} mbar
- Ultra high vacuum (UHV) 10^{-7} - 10^{-12} mbar
- Extreme vacuum (XHV) $< 10^{-12}$ mbar

The pressures at which the ALPHATRAP experiment will operate range from the about 10^{-11} mbar to below 10^{-15} mbar expected at the trap chamber, while the pressures under which the cryogenic vacuum valve was tested range between 10^{-3} mbar to 10^{-8} mbar.

Depending on the characteristic dimensions of a vacuum system through which the gas is flowing (typically given as the cross section of the tubing) and the pressure, three main types of the gas flow can be identified :

- **Continuum Flow** At high pressures, the mean free path of the gas particles is small compared to the cross section of the tubing. Collisions of particles between each other dominate over collision with the walls.
- **Molecular Flow** When pressure is low enough, the mean free path of the particles becomes larger than the cross section of the tubing. In this case, collisions between the particles are so rare that they can be ignored, predominant collision are between the particle and the walls of the vacuum system. It can be considered that the particles travel independently of other particles and interact only with the walls.
- **Transitional Flow** In the intermediate pressure range, the particle-particle collisions are as frequent as the particle-wall collisions, both of these collisions determine the flow characteristics. This type of flow is encountered in a transition region between continuum and molecular flow, e.g. when pumping down the vacuum system.

The above listed flow types can be identified by using a dimensionless Knudsen number Kn . The Knudsen number is defined as the ratio of the mean free path l and the characteristic dimension d of the component through which the gas is flowing

$$Kn = l/d. \quad (3.5)$$

For tubes of circular cross section, d is just the tube diameter. From the Knudsen number three types of flow can be identified, found in [Jou08], which are listed in the table below.

Knudsen number	Type of flow
$Kn > 0.5$	Molecular flow
$0.5 > Kn > 0.01$	Transitional Flow
$Kn < 0.01$	Continuum flow

The boundaries defined by the Knudsen number between continuum, molecular and transitional flows serve more as a rule of thumb rather than firmly set boundaries in determining the flow type. The gas flow can be described in many ways, however,

two definitions commonly used are the pumping speed S and the throughput Q . The pumping speed is defined as the volume flow rate

$$S = \frac{dV}{dt}, \quad (3.6)$$

and is typically expressed in units of l/s. The throughput is defined as

$$Q = p S = p \frac{dV}{dt}, \quad (3.7)$$

where p is the pressure. Q is typically expressed in the units of mbar l/s. Both of these definitions for the gas flow are volumetric flow rates, they do not give information on the quantity of gas flowing unless temperature is defined. By defining the temperature, throughput can be converted to the number of gas particles flowing per unit time by using the ideal gas law [Jou08] as follows

$$Q_N = \frac{dN}{dt} = \frac{d}{dt} \left(\frac{pV}{k_B T} \right) = \frac{1}{k_B T} p \frac{dV}{dt} = \frac{Q}{k_B T}, \quad (3.8)$$

where Q_N is now a particle flow rate. In a similar way, the mass flow rate and the molar flow rate of the gas can be found [Jou08]. It is important to note that in a steady state, the throughput Q will have the same value at every point in the vacuum system. This is based on the fact that quantity of gas entering in to the vacuum system/component must eventually come out, since the number of particles must be conserved. In practice, this means that if a steady gas flow rate is established while the volume and the temperature are held constant, it is possible to estimate the pressures at every point in the system. Provided that the geometry of the system is not complicated the calculating these estimates is relatively easy. Connection of the vacuum system geometry to the gas flow and the pressure is described in the following.

The flow of gas through a component of the vacuum system is related to the pressure drop across the component and the property of that component known as the conductance C . The conductance is defined by the following relation

$$Q = \frac{C}{p_2 - p_1}. \quad (3.9)$$

In molecular flow regime, the conductance is independent of the pressure and for a given gas depends only on the geometry of the components and temperature. Hence, by measuring the pressure difference at a known gas throughput the conductance of a component can be found. It should be noted that the relation Equation 3.9 assumes the pressures p_1 and p_2 are measured in a larger chambers connected to the each end of the component. Conductance relations (in molecular flow regime) for some of the typical geometries found in vacuum systems are given in the following.

The conductance for an aperture, found in [Rot12], is given by

$$C = 3.64 \sqrt{\frac{T}{M}} A, \quad (3.10)$$

in l/s units, where A is the area of the aperture in cm^2 , T is the temperature and M is the molar mass in g/mole. The conductance of the tube of length l and diameter d is given in [Rot12], where it is assumed that that $l \gg d$ is given by

$$C = 3.81 \sqrt{\frac{T}{M}} \frac{d^3}{l}, \quad (3.11)$$

in l/s units, where T and M are the same as in Equation 3.10. For the short tubes, the conductance of the entrance will have a significant contribution, using 3.9.2 instead gives an overestimated result [VR10]. For combination of components the total conductance C_T can be found from the following rules

- Series connection of components

$$1/C_T = 1/C_1 + 1/C_2 + 1/C_3 \dots \quad (3.12)$$

- Parallel connection of components

$$C_T = C_1 + C_2 + C_3 \dots \quad (3.13)$$

The relations above are strictly valid only when components are considered independently. Equation 3.12 assumes that the components are separated from each other by a larger volumes, which allows the particles velocities to acquire the Maxwell-Boltzmann distribution. For example, connecting two identical tubes in series, directly one after another, would result in a greater total conductance than predicted by Equation 3.12 [O'H05, CC05]. The reason is that the velocity distribution of the particles inside the tubes is not in accordance with the Maxwell-Boltzmann distribution. Most of the particles will have a larger velocity component along the tubes axially. Hence, it will be "easier" for particles to pass from one tube to the other than if the tubes are connected through a large chamber. Equation 3.13 assumes that there is no interference between the inlet flows of the components, which is not the case when inlets of the components are close to each other [Jou08][Jou08]. Therefore, both equations are useful when estimates are good enough as a solution and should be used with caution when accurate analysis of the conductance has to be made.

When a vacuum chamber is pumped out by a vacuum pump of speed S , connected to the chamber through a tubing of conductance C_t the effective pumping speed S_{eff} at the chamber is given as

$$\frac{1}{S_{\text{eff}}} = \frac{1}{S} + \frac{1}{C_t}. \quad (3.14)$$

From this relation follows that the tubing conductance C_t will determine the available pumping speed at the chamber if the pumping speed S is significantly higher than the tubing conductance. When discussing pumping effect involving cryo-cooled surfaces it is often useful to define an area related pumping speed. This can serve to estimate the pumping speed related to the surfaces held at cryogenic temperatures. The area related pumping speed of an aperture is defined a

$$S_P = c \cdot C_{ap}, \quad (3.15)$$

where C_{ap} is the conductance of an aperture defined by relation Equation 3.10 and c the sticking probability of the gas particle to the surface. For absolute sticking c has a value of 1, meaning that particles arriving at the surface are completely removed from the vacuum system.

3.3. Analytical modeling

A high-precision measurement of the electron g -factor in highly-charged ions demands sufficiently long lifetime¹ (storage-time) of the ion. From the moment when the ion is trapped, carrying out the measurement will require a minimum of about one week in the ALPHATRAP experiment [Stu13]. This gives a lower limit for the lifetime of trapped ions which will be discussed in the following.

The main loss process of highly-charged ions is through charge exchange with the neutral rest-gas particles [Her99]. In order to assess the ion lifetime it is necessary to estimate the vacuum conditions that can be achieved in the trap-chamber. The rest-gas pressure expected in the trap-chamber (without the valve) can be estimated from considering a schematic model of the ALPHATRAP setup shown in Figure 3.1. When the setup is operational, the pressure at the point where the beam-line enters the 4 K temperature stage is expected to be on the order of 10^{-11} mbar.

¹Terms lifetime and storage-time are here used interchangeably.

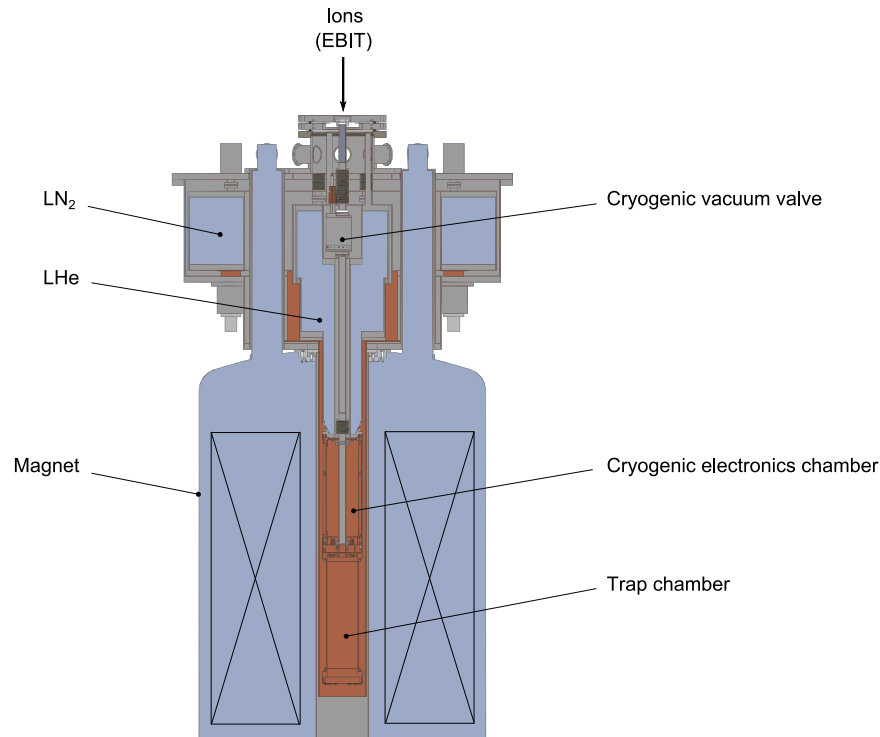


Figure 3.1.: Schematic view of a cross-section through the superconducting magnet and the inner cryostat of the ALPHATRAP setup. Location of the cryogenic vacuum valve, the trap chamber and the detection electronic chamber in the experimental setup are shown.

From that point, the trap-chamber below is connected through a tube segment with a length of 89.5 cm and a diameter of 1.6 cm, where a material with high absorption properties is located. This creates a cryopumping effect. Gases with negligible vapor pressure at 4 K will be pumped by cryo-condensation, while a group of gases with relatively high vapor pressure even at 4 K (like H_2 and He) can be efficiently pumped by cryosorption on the high absorption properties material. The structure of the charcoal consisting of a vast number of micro-pores represents a large surface for these gas particles even if adsorption occurs only in one mono-layer. Since the rest-gas particles must pass through a 77 K stage and then through a tube at 4 K stage, it is expected that most of the rest-gas will be removed by cryo-condensation even before reaching the trap-chamber. Hence, it can be taken that the rest-gas in the trap-chamber consists only of hydrogen and helium.

From above considerations, the trap-chamber can be regarded as a cryopump with an inlet of 1.6 cm diameter pumping out the volume at constant pressure of $\sim 10^{-11}$ mbar through a tube. The conductance of the tube segment C_t can be found by using Equation 3.11, which gives $C_t = 0.178$ l/s (He, 4 K). Provided that there is

no back-streaming of the rest-gas particles from the inlet of the trap-chamber to the beam-line, that is if every particle is caught either by means of cryo-condensation or cryosorption, the pumping speed S_{tc} of the trap-chamber can be found according to Equation 3.15. Setting the trapping coefficient to $c = 1$ (absolute sticking) and using the inlet aperture of the trap-chamber with the same diameter of 1.6 cm as the tube segment for the area A gives $S_{tc} = 7.52$ l/s (He, 4 K). Since the trap-chamber is connected through the tube of conductance C_t to the volume at 10^{-11} mbar, the pumping speed S_{tc} will be reduced at that point to the effective pumping speed S_{eff} , which can be found using Equation 3.14 as

$$\frac{1}{S_{eff}} = \frac{1}{S_{tc}} + \frac{1}{C_t}. \quad (3.16)$$

The pressure in the trap-chamber can now be estimated using the basic assumption of the gas-flow theory. In a steady state the throughput $Q = p S$ must be the same at all points in the vacuum system, hence

$$Q = 10^{-11} \cdot S_{eff} = p_{tc} \cdot S_{tc}, \quad (3.17)$$

from which trap-chamber pressure p_{tc} follows

$$p_{tc} = \frac{S_{eff} \cdot 10^{-11}}{S_{tc}} = \frac{10^{-11} \cdot C_t}{S_{tc} + C_t}. \quad (3.18)$$

Inserting the values for S_{tc} and C_t gives $p_{tc} = 2.3 \times 10^{-13}$, calculated for helium, C_t and S_{tc} for H_2 gives irrelevant difference for this discussion. Therefore, it can be expected that the trap-chamber pressure will have about 10^3 times lower pressure relative to the point where the beam-line enters the 4 K temperature stage.

In order to evaluate the vacuum conditions in the trap-chamber required for trapping of highly-charged ions, it is necessary to know how the rest-gas pressure affects the ion lifetime. This can be estimated from result found in [Her99], where the ion lifetime and the rest-gas pressure are related by the equation

$$p = \frac{1}{\sigma \tau} \sqrt{\frac{\frac{1}{3} k_B T}{\frac{1}{m_{gas}} + \frac{1}{m_{ion}}}}. \quad (3.19)$$

The σ , τ , m_{gas} , m_{ion} are the charge exchange cross section, the ion lifetime, the mass of the rest-gas particle and the mass of the ion, respectively. For the charge-exchange cross section σ , the empirical relation found in [Man86] can serve as an estimate

$$\sigma_{q,q-1} = 1.43 \cdot 10^{-12} \cdot q^{1.17} \cdot I_p^{-2.76}. \quad (3.20)$$

Where q is the charge state of the ion and I_p the ionization potential of the rest-gas particle. Hence, the loss process takes place when the ion acquires the electron

from the rest-gas particle. Equation 3.19 allows now to express the ion storage times (ion lifetime) as a function of the pressure and the charge state of the ion. Figure 3.2 shows an ion storage times in dependence of the charge state and the rest-gas pressure, where hydrogen and helium are taken as the rest-gas at temperature of 4 K. The red dashed line marks a one week of storage time which is a minimum required storage time as discussed above.

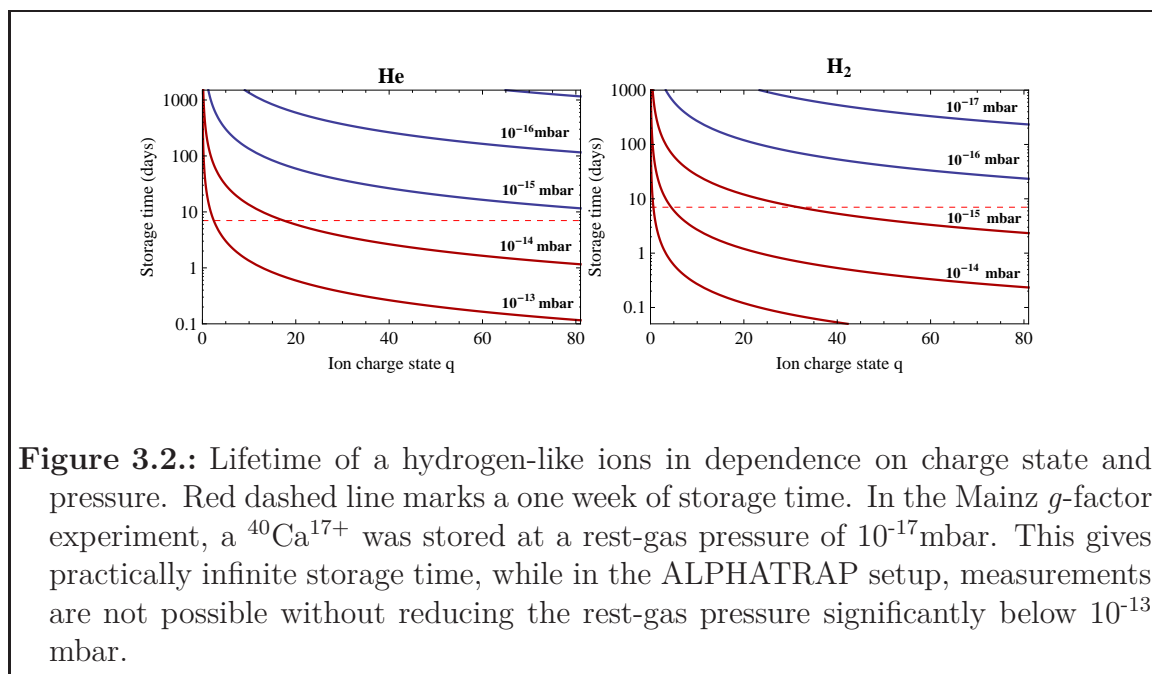


Figure 3.2.: Lifetime of a hydrogen-like ions in dependence on charge state and pressure. Red dashed line marks a one week of storage time. In the Mainz g -factor experiment, a $^{40}\text{Ca}^{17+}$ was stored at a rest-gas pressure of 10^{-17} mbar. This gives practically infinite storage time, while in the ALPHATRAP setup, measurements are not possible without reducing the rest-gas pressure significantly below 10^{-13} mbar.

From the results presented in Figure 3.2 and the minimum time required for the measurement process, it can be seen that for a pressure of 10^{-13} mbar, the storage times are practically below one day even for low charge states. For the ALPHATRAP experiment, aiming to trap highly-charged ions, this means that the g -factor measurements are not possible without reducing the trap-chamber pressure well below 10^{-13} mbar. To enable measurements on highly-charged ions the trap-chamber pressure should be reduced to approximately below 0.5×10^{-16} mbar where the storage times above the critical limit of one week for all charge states could be attainable. The expected pressure in the trap-chamber of 10^{-13} mbar should be reduced by a factor of above 500 to achieve a sufficient vacuum for the experiment. Equation 3.18 gives suggestions on how to achieve this reduction. If it is assumed that the pressure at the point where the beam-line enters the 4 K stage and the inlet aperture area of the trap-chamber are set by the setup construction requirements, the only way to reduce the pressure in the trap chamber is by reducing the conductance of the tube segment. The effect of the conductance reduction on the trap-chamber pressure can be then found from the ratio

$$\frac{p_r}{p_{tc}} = \frac{S_{tc} + C_t}{r \cdot S_{tc} + C_t}, \quad (3.21)$$

where p_r is the trap-chamber pressure with a conductance reduced by a factor of r . Hence, it can be seen that the conductance reduction by a factor about $10^2 - 10^3$ gives the same factor in the reduction trap-chamber pressure reduction (for S_{tc} and C_t calculated above). The above discussed requirement of the conductance reduction is a motivation for a cryogenic vacuum valve for the ALPHATRAP setup. By reducing the conductance in between the trap-chamber and the point where the beam-line enters the 4 K section of above 500, the valve enables sufficiently low vacuum and therefore trapping and storing of highly-charged ions for the measurement process.

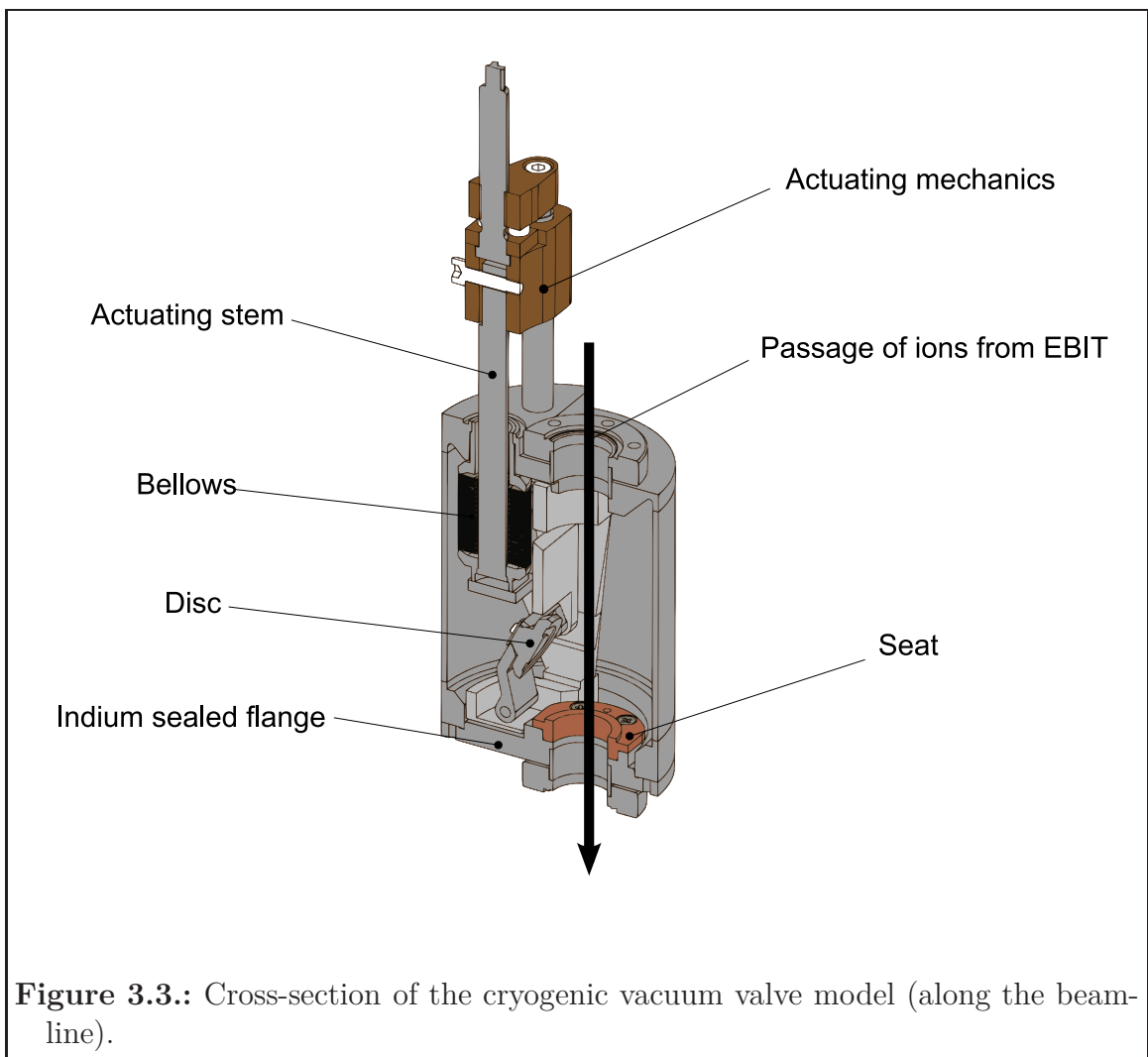
3.4. Mechanical design

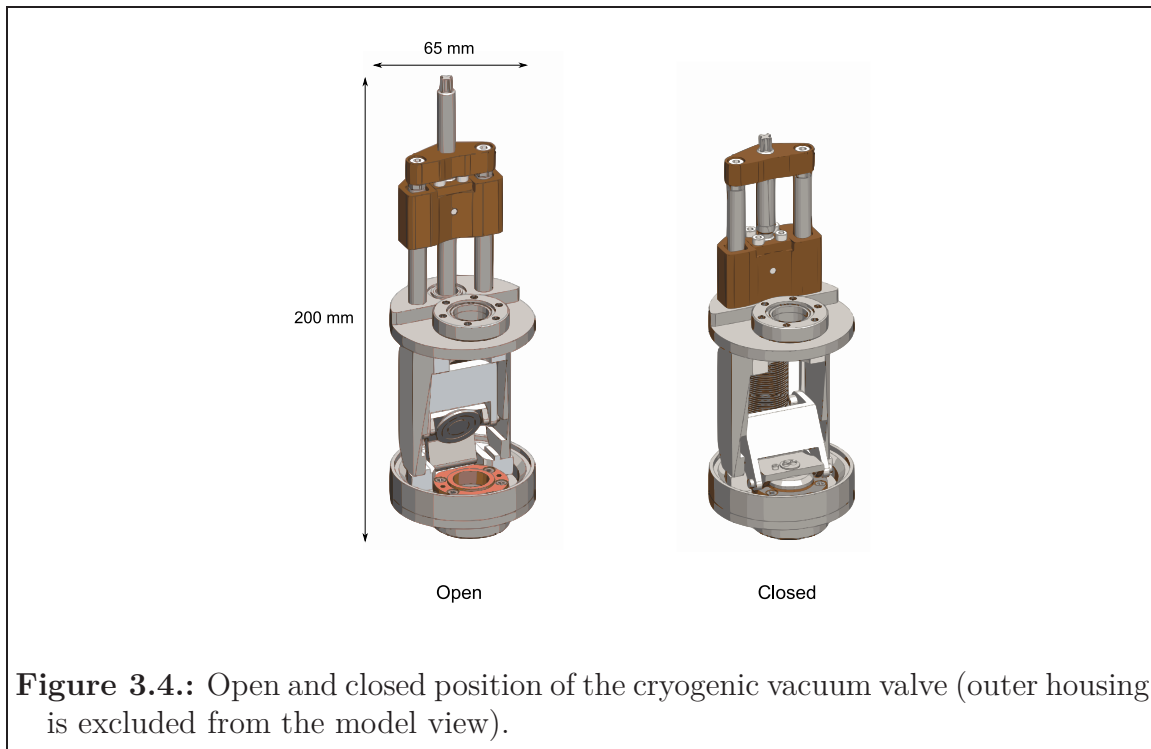
Position of the cryogenic vacuum valve in the experimental setup is shown in Figure 3.1, where the superconducting magnet and the liquid helium/nitrogen cryostat dewars are shown in a cross-section view. The valve is situated in an insert of the liquid helium dewar at the top. This position ensures that the valve thermalizes to the same temperature as the beam-line section and the trap chamber below the valve at 4.2 K temperature. This provides a better reduction of the external rest-gas flow into the trap chamber. The beam-line channel connects to the valve through a shielding that encloses the two cryostat dewars at the top, and after the valve, continues down to the trap chamber via 89.5 cm long tube of 1.6 cm in diameter. The valve is actuated by using a rotary feed-trough connected to the actuation mechanism on the top of the valve housing. The feed-through extends outside trough the cryostat shielding enclosure to the room temperature from where the valve is actuated.

The actuation can be controlled manually or automatically (e.g. by using a motor), the shut-off time of the valve by using manual actuation is ~ 30 seconds. Thermal contact of the valve to the room temperature over the rotary feed-trough can be disconnected, thereby reducing thermal load on the liquid helium cryostat and thus consumption of helium. Cross-section of the valve model in Figure 3.3 shows internal parts and mechanics of the valve. The interior of the valve is sealed off from the actuating mechanism outside by a stainless-steel bellow², which are welded at the bottom to the actuating stem and at the top to the valve housing. When the valve is in open position the bellows are compressed, while they are expanded when the valve is in closed position. Bellows are the most sensitive component of the valve and their bending or torsion should be avoided, the actuating stem is therefore supported by a guiding frame allowing only vertical (up/down) movement. This movement is transferred by means of two lever mechanism to the valve disc. When the valve closes, the disc is pressed into the seat sealing off the trap chamber, and in open position the disc completely clears the beam-line passage for the ions. The disc is not rigidly fixed, but has a certain play ensuring that the surfaces of the disc and the seat are in parallel alignment when the valve is closed. Access to the inner parts

²Edge welded bellow

of the valve is made possible by opening the indium sealed flange at the bottom of the housing, which is also used to assembled/disassembled internal mechanics. The valve is mounted in the beam-line by using CF16 flanges on the inlet and the exit side of the valve serving also as mechanical fixtures. Since the torque produced by actuating the valve is transferred to the beam-line tubing (The LHe cryostat hangs by a three G10 rods from the shielding top, so the torque is transferred to these rods first), the valve is designed to be operable by using sufficiently low torques that do not endanger the experimental setup. Figure 3.4 shows a model of the valve in an open and closed position with approximate height and diameter measures. The photograph of the valve is shown in Figure A.1.





3.5. Conductance of the cryogenic vacuum valve

The intrinsic conductance of a component is given as a product of the aperture conductance through the entrance plane C_A and transmission probability factor a which depends only on the geometry under molecular flow condition [Jou08]. Therefore, for mechanical components of vacuum system, such as valves, the only way to reduce the conductance is by changing the geometry through which the gas is flowing³. Since the valve operates by reducing the inlet area to the rest-gas flow by applying pressure between two metal surfaces, the following section will discuss how conductance reduction is affected by the parameters that characterize the two sealing metal surfaces in contact (or proximity). Models for the sealing interface of the cryogenic vacuum valve and calculation of the corresponding conductance reductions are presented.

The mechanical design of the cryogenic vacuum valve, presented in section 3.4, gives a starting point for the evaluation of the conductance of the closed valve. Considering that the distance between the valve disc and the seat is in the order of less than 100 μm , the sealing interface will have the dominant contribution to the total conductance of the valve. Therefore, this section will only discuss conductance geometries related to the sealing interface of the valve, as this value will characterize the total performance. The conductance of the open valve will not be discussed, since in the open position the valve does not contribute significantly to the vacuum attained in the system.

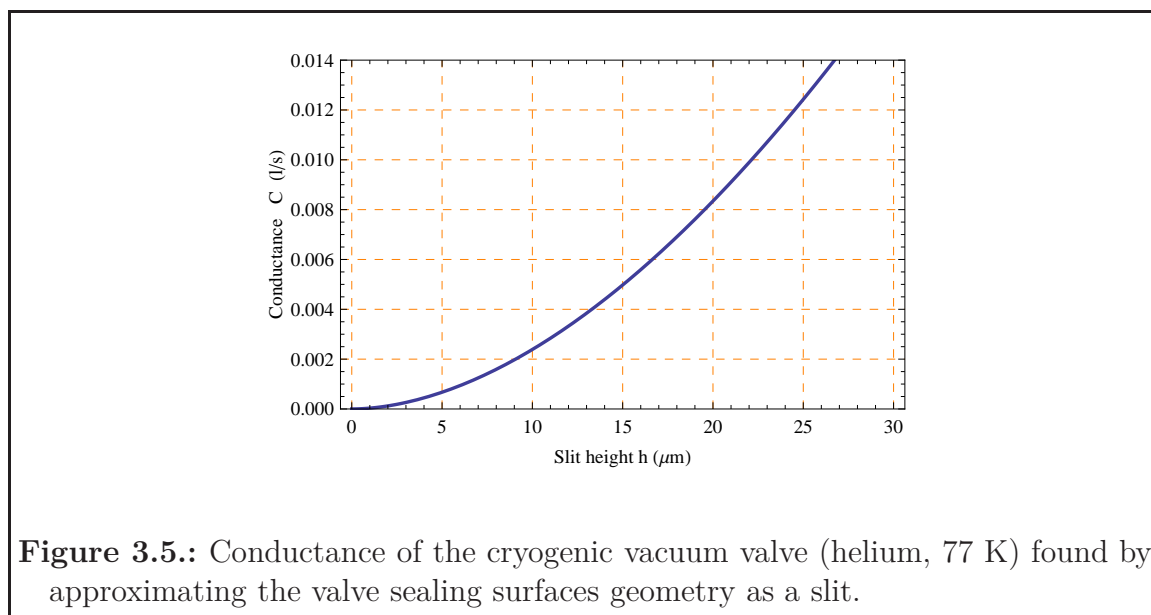
³Assuming fixed temperature

3.5.1. The slit model

In the simplest way, the conductance of the valve sealing interface can be roughly estimated by assuming that the space between the disc and the seat in closed position has a slit-like shape. The length of the slit can be taken as the difference between inner and outer radius of the seat contact surface (0.25 cm), and the width of the slit as the mean circumferential sealing length (5.8 cm). For the slit height, a reasonable assumption is that it could take values from around 10 μm to 30 μm , since the sealing surface roughness is approximately 16 μm . The slit height above 30 μm may correspond to a case when the contacting surfaces are not closing properly⁴. The conductance of a slit-like, thin rectangular pipe, which can serve as an approximation to the sealing interface geometry described above, can be found in [Ber65, O'H05], it is given by

$$C = a \cdot \frac{v_{av}}{4} A, \quad (3.22)$$

where a represents the transmission probability factor, v_{av} is the average thermal velocity of the particles and A is the entrance area of the slit (C in m^3/s units). The average velocity v_{av} can be found from Equation 3.2, while the transmission probability factor a for our geometry can be found in section A.1 by using $b = 5.8$ cm and $l = 0.25$ cm for the slit width and length respectively. Figure 3.5 shows the conductance when the valve sealing interface is approximated by the slit geometry with dimensions given above for helium gas at 77 K temperature.



As can be seen from the figure, for the slit height of about ~ 16 μm the conductance is ~ 0.005 l/s. This corresponds to a factor ~ 150 in conductance reduction at 4 K

⁴Larger irregularities on the surfaces like foreign particles, mechanics fault and misalignment between the sealing surfaces.

relative to the tube segment conductance C_t discussed in section 3.3. To achieve a factor of above 500 the slit height of about less than $8 \mu\text{m}$ is needed. This suggests that it could be possible to reach the needed conductance reduction if larger surface irregularities are ruled out, and if the roughness of the sealing surfaces is sufficiently reduced considering to the $\sim 8 \mu\text{m}$ obtained by the slit model. Since the slit model approximates the circular geometry of the sealing interface and does not take the surface micro-structure nor the sealing forces into account it can only serve as a rough estimate. Nonetheless, it can be at least be a useful reference point for further analysis.

3.5.2. The sealing interface model

A model of the sealing interface which takes micro-structure and the sealing forces into consideration, can be found in [RI67]. The model assumes that the two contact surfaces are characterized by their surface roughness and waviness, as shown in Figure 3.6. The total waviness of the sealing surfaces is on the softer surface (upper surface) and the total roughness is represented on the harder surface (lower surface). The sealing process is considered to consist of three stages. The accommodation stage, the normal sealing stage and the local sealing stage. The accommodation stage starts when the sealing surfaces are brought into contact by using just contact forces. In that stage the conductance is determined by the waviness and the roughness (Figure 3.6 a)). By applying a force on the sealing surfaces the initial waviness a_{m0} will decrease until $a_{m0} = 0$ and the softer surface is flattened out (Figure 3.6 b)). At that point the accommodation stage ends and the conductance is determined just by the surface roughness A . At a further increase of the force, the normal sealing stage begins, which is not shown in Figure 3.6. In that stage the harder material interpenetrates in the softer one, and the conductance is determined by the interpenetration depth.

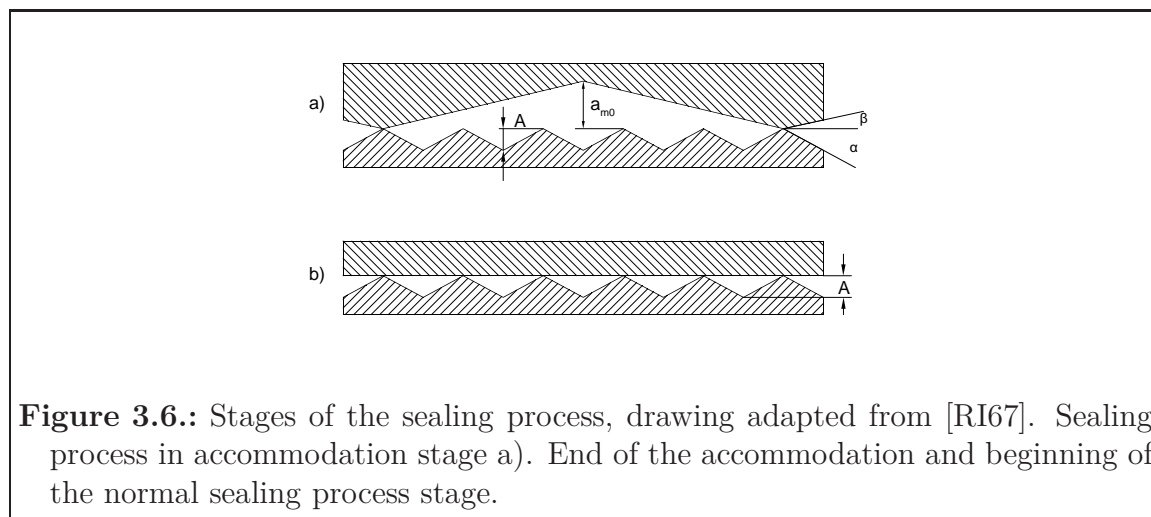


Figure 3.6.: Stages of the sealing process, drawing adapted from [RI67]. Sealing process in accommodation stage a). End of the accommodation and beginning of the normal sealing process stage.

Since the local sealing stage requires much higher forces than produced when closing the cryogenic vacuum valve, it will be left out from discussion. To estimate the stage of the sealing process, the concept of tightening index defined as

$$k = P/R = F/(LwR), \quad (3.23)$$

can be used [Rot12]. F (kg) is the applied force, L (cm) is the mean circumferential sealing length (cm), w (cm) is the radial width of the seal interface and R (Kg/cm²) is the material dependent sealing factor of the softer material. The sealing factors for various metals are given in [Rot12], which are found with respect to helium gas at 25° C temperature. However, they can be used to give an estimate of the upper limit for the tightening index of the cryogenic vacuum valve. Taking the force used for closing the cryogenic vacuum valve on the order of 10N, the dimensions of the sealing interface ($L = 5.8$ cm, $w = 0.25$ cm) and choosing the sealing factor of the copper seat as $R = 250$ kg/cm² (corresponding to the softer copper gasket), gives the tightening index of 2.8×10^{-3} . Since it was found [Rot12] that the accommodation stage of the sealing process extends typically up to a tightening index k of ~ 0.5 to 0.6 , it can be further considered that the sealing process in the valve occurs mainly in the accommodation stage. In support of this come further considerations:

- The sealing factor of 250 kg/cm² is more appropriate to use with a softer material ring-type flexible gaskets, where the waviness is easier to overcome [Rot12, RI67]. The sealing factor of the solid material, like the copper seat of the cryogenic vacuum valve is expected to have a higher R value.
- R depends on the temperature [RI67]⁵ and the hardness of the material [Rot12]. Hence, it is reasonable to expect that the overall change from the room to the cryogenic temperatures is toward higher values of R .
- Increase of the force by an order of magnitude for the same sealing surface geometry as above, and using $R=250$ kg/cm² gives ~ 0.028 for the tightening index k . This is still about five times less than typically needed for the sealing process to leave the accommodation stage.

From the discussion above, it can be assumed that the a_{m0} parameter, which describes the waviness in the accommodation stage, will not be significantly reduced by applying force and always have its initial value. Therefore, the sealing process in the valve will always be at the starting point of the accommodation stage.

A model suitable for the description of the accommodation sealing stage is given in [RI67] by relation

$$C_a = C_0 \cdot F\left(\frac{a/2}{A}\right), \quad (3.24)$$

where C_0 corresponds to a conductance at the point between the accommodation stage and the normal sealing stage (Figure 3.6 b)). The function $F((a/2)/A)$ describes the waviness and it is given in section A.1. A is defined as peak-to-valley

⁵Functional dependence of R on temperature was not given in the article.

height of the surface roughness, and a as the distance between the sealing surfaces caused by waviness during accommodation stage. Since the model assumes that the angles associated with the surface roughness A and the initial waviness a_{m0} are small, indicated as α and β in Figure 3.6, for the purposes considered here it can be taken that $F((a/2)/A) = F((a_{m0}/2)/A)$, as shown in [Rot12]. The function $F((a_{m0}/2)/A)$ is used here taking $\alpha = 4^\circ$, since it was found [Rot12] that on machined surfaces slopes of the peaks corresponding the surface roughness A almost completely have values between 1° and 4° . For an annular type of seal, as our, the function C_0 was found [RI67] to be

$$C_0 = 1.93 \times 10^4 \sqrt{\frac{T}{M}} \frac{2\pi}{8.12} \frac{A^2}{\ln(r_0/r_i)}, \quad (3.25)$$

where r_0 and r_i are the outer and the inner radius of the annular sealing surface (C_0 in cm^3/s). In the case of cryogenic vacuum valve, r_0 and r_i are 1.05 cm and 0.8 cm respectively (dimensions of the seat surface) and the surface roughness A is approximately $\sim 16 \mu\text{m}$. The waviness parameter a_{m0} is not know, however Equation 3.24 can be plotted with a_{m0} as a parameter, which allows to assess the conductance of the closed valve. Figure 3.7 shows the conductance of the closed valve depending on the surface roughness A of the sealing surfaces and the waviness characterized by the a_{m0} parameter at 77 K temperature for helium.

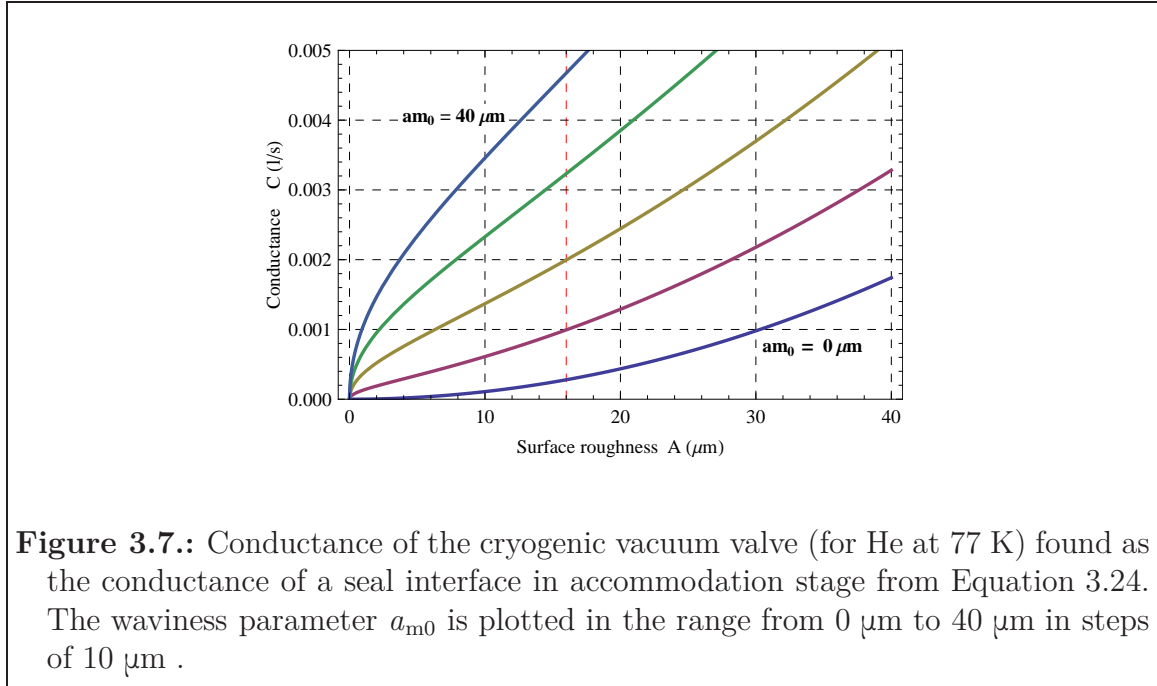


Figure 3.7.: Conductance of the cryogenic vacuum valve (for He at 77 K) found as the conductance of a seal interface in accommodation stage from Equation 3.24. The waviness parameter a_{m0} is plotted in the range from $0 \mu\text{m}$ to $40 \mu\text{m}$ in steps of $10 \mu\text{m}$.

If the surface roughness is about $\sim 16 \mu\text{m}$ the conductance for $a_{m0} = 0$ (no surface waviness) is $\sim 3 \times 10^{-4} \text{ l/s}$, which can be taken as theoretical minimum. For a more realistic assessment a_{m0} should be greater than zero. From the slit model, discussed in the previous section, it was found that for $A \sim 16 \mu\text{m}$ the conductance is $\sim 0.005 \text{ l/s}$. Since the surface roughness is not considered by the slit geometry, it can be

assumed that the slit model gives upper value of the valve conductance. This upper conductance value is obtained here for waviness a_{m0} of $\sim 42 \mu\text{m}$.

3.6. Test results

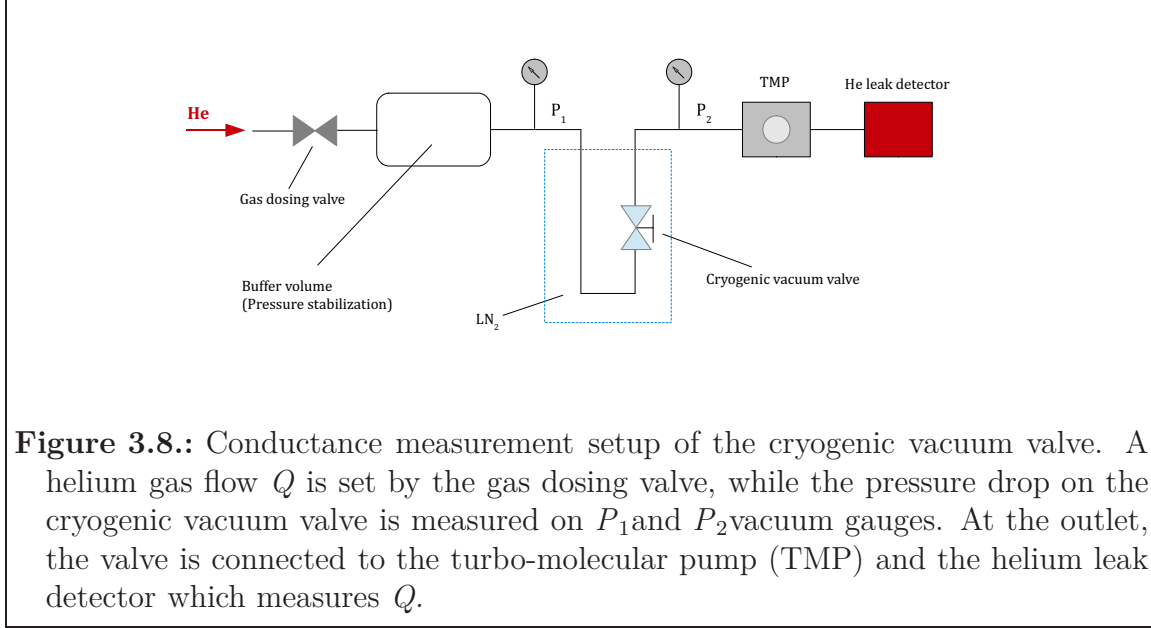
3.6.1. Measurement setup and procedure

Vacuum valves are typically characterized by their conductance in completely open position, since it is preferable to have a high conductance for a gas flow when a valve is opened. For the cryogenic vacuum valve, the conductance in the open position is not as important as the conductance in the closed position. The open position is needed for the ion injection, therefore the conductance is irrelevant here. On the other hand, when the ion is trapped, the closed valve should create a "resistance" for the rest-gas flowing into the trap chamber. The purpose of the measurements described in this section is to determine the conductance of the cryogenic vacuum valve in the closed position.

Analytical calculation of the gas flow conductance's of complex geometries like valves or a valve sealing interface is not possible [Jou08], the only way to obtain them is through estimations or by using measurements. The conductance measurement process is generally performed by using an intrinsic or reduced conductance measurement [Jou08], which depends on how the test object is mounted in the test setup. The measurement of the intrinsic conductance is obtained when the component is mounted between two separated volumes in a larger vessel, while the reduced conductance measurement occurs in the case when the component is mounted in between the tubing having the same diameter as the inlet/outlet of the component. For reliable tests, the conductance of the valve has to be measured at cryogenic temperatures. This enables to assess the effects on the mechanics due to the cool down on the valve performance. Measuring intrinsic conductance of the valve in that way would be very difficult to implement and can be excluded as an option. The reduced conductance measurement, on the contrary, is relatively easy to construct together with the requirement that the valve must be operated at cryogenic temperatures. The drawback is that the conductance must be later deduced from the assembly conductance. In this case, the flanges and the tubing that are connected to the component could give a higher error in the conductance measurement.

Due to the discussion above, the measurement setup for the conductance of the cryogenic vacuum valve is based on the reduced conductance scheme, shown in Figure 3.8. The gas throughput Q is set by a dosing valve which can produce flow rates down to 10^{-7} mbar l/s. Helium, which is used as a testing gas, flows into a large vessel used to stabilize the pressure in the system and enabling a steady throughput. The cryogenic vacuum valve is situated within the liquid nitrogen cryostat over which the pressure difference ($P_1 - P_2$) is measured by two vacuum

gauges. The outlet of the valve is connected to the turbo-molecular vacuum pump (TMP), which is eventually connected to the helium leak detector measuring the throughput Q . The measurement procedure starts with the valve initially in the open position and setting the helium flow through the dosing valve. Eventually, when the steady-state is established and the throughput and the pressure show a certain consistency, the cryogenic vacuum valve is closed. This is done from above the liquid nitrogen cryostat by using a G10 rod mounted on the actuating mechanism of the valve. Closing the valve causes the system to go into a transition state which can last from a couple of hours up to a day, depending on the set flow rate.



After the transition period the system re-establishes steady-state with the new pressures on the vacuum gauges while the throughput Q stays constant (ideally). During the entire process, the throughput and the pressures are logged via an automated data-acquisition software. From analyzing the collected data, the conductance of the vacuum line between the two pressure gauges C_L can be found from Equation 3.9 given above. The conductance of the closed valve is estimated from the relation for components connected in series, Equation 3.12, as

$$\frac{1}{C_L} \approx \frac{1}{C_{CV}} + \frac{1}{C_T}, \quad (3.26)$$

where C_T is the conductance of the tubing connected to the valve. Since the mechanical properties of the valve will not change significantly from 77 K to 4 K temperature, the measurement at liquid-nitrogen temperature also ensures that the valve will operate at a temperature of 4 K. The conductance in molecular flow regime scales as

$$C \sim \sqrt{\frac{T}{M}}, \quad (3.27)$$

where T is the temperature and M is the molar mass of the gas. Therefore, the conductance of other gases can be found from the measured conductance of helium

$$C_x = C_{He} \sqrt{\frac{M_{He}}{M_x}}, \quad (3.28)$$

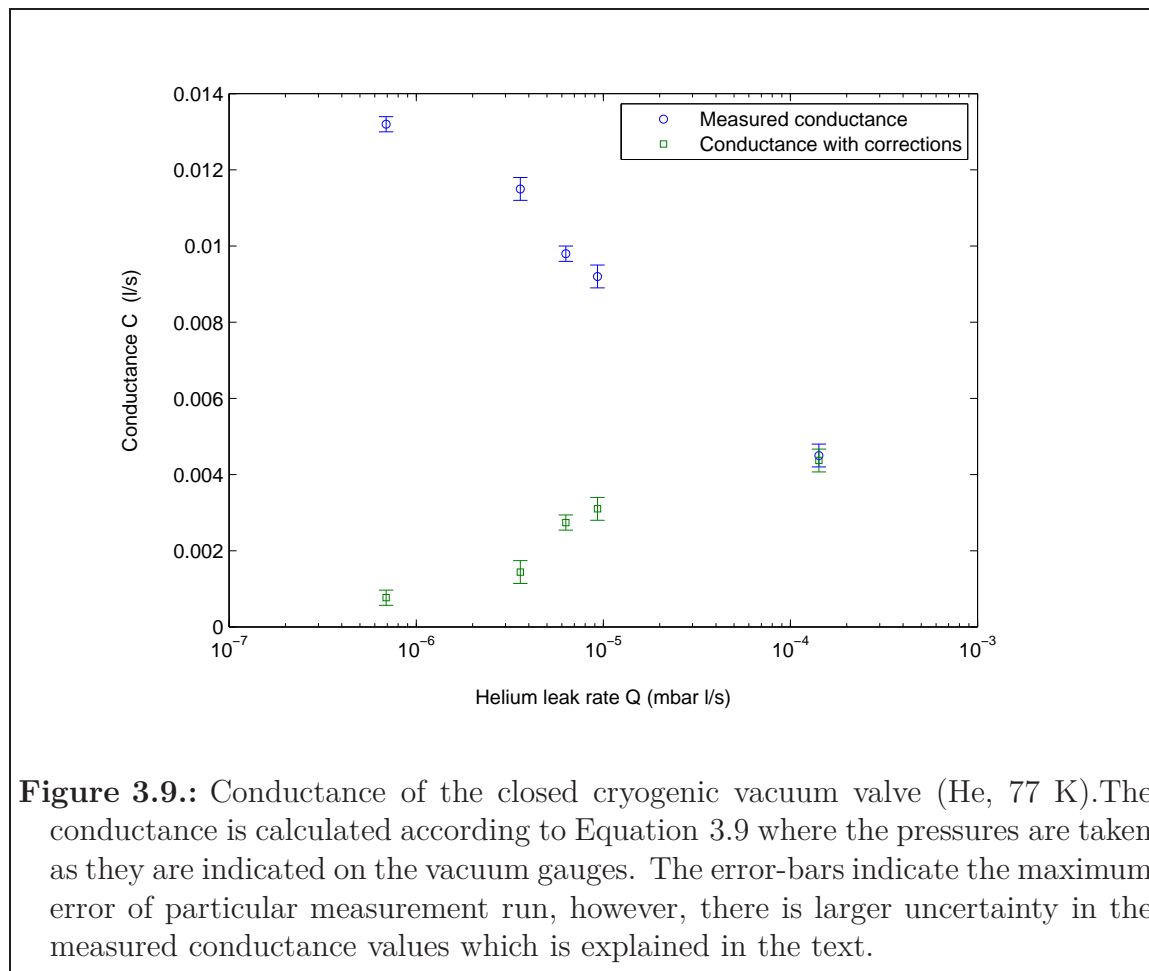
where C_{He} is the conductance of the valve found for helium, M_{He} is the molar mass of helium and the index x designates the gas for which the conductance has to be found. In the same way, the conductance of the valve at a temperature of 4 K can be found.

3.6.2. Conductance measurement results

The cryogenic vacuum valve conductance measurements lasted about a month, whereby the individual measurements runs spanned from about 4 to 70 hours. The valve was once taken out from the setup to adjust the internal mechanics and refine the sealing surfaces by milling and polishing. Thereafter, the valve was inserted back in setup for the remaining measurements. Figure 3.9 shows the conductance measurement results.

One characteristics that is seen in the measured data presented above is that the conductance C decreases as the leak rate Q increases. The decrease of the conductance with the increase of the leak rate is inconsistent with the theory, since conductance in molecular flow regime depends only on the geometry and the temperature (for a certain gas). With increasing the pressure, the gas flow could go from molecular toward viscous flow regime in some parts of the vacuum system, but this can only result in a higher values for the measured conductance, since conductance increases in that direction[Jou08]. After completing the conductance measurements the vacuum gauges have been tested. Using a pressure rate-of-rise test method, it was found that the indicated pressure from $\sim 10^{-6}$ up to $\sim 6 \times 10^{-3}$ mbar strongly deviates from the expected linear. Especially in the lower range, the indicated pressure was too low. This can explain the relatively high conductance obtained at measurements with low leak rates around 10^{-6} - 10^{-6} mbar l/s. When the cryogenic vacuum valve is closed, these leak rates produce a pressures in the range where the indicated gauge pressures are too low, and hence, give a higher conductance values. Therefore, the corrected conductance in Figure 3.9 was obtained by correcting the measured pressures, according to the data obtained from the rate-of-rise tests, and applying the vacuum gauge conversion factors for the helium.

The corrected conductance data points in the figure do not show an increase of the conductance with the increase in the leak rate, which is in agreement with theory (for



molecular flow conditions). All data points below the leak rate of 10^{-4} mbar l/s are shifted down, since these measurements are conducted at higher effective pressures than indicated by the vacuum gauges. The data points above the leak rate of 10^{-4} mbar l/s are not significantly affected by the corrections. These measurements are conducted at a relatively high pressure (above $\sim 10^{-3}$ mbar) where the vacuum gauges shows the correct indicated pressures⁶, and the helium conversion factor of the gauge are small. Before assessing the valve conductance one more point must be noted. Following the last measurements, a background signal of $\sim 10^{-8}$ mbarl/s was indicated on the leak detector although the helium dosing valve was completely closed. A test performed with the vacuum gauges showed that by turning off the gauges, the background signal could be decreased by approximately one order of magnitude. If however a helium leak rate of $\sim 10^{-7}$ mbar l/s was set by the dosing valve⁷, turning off the gauges resulted in an increase of the leak rate. At leak rates of above $\sim 5 \times 10^{-6}$ mbar l/s turning the vacuum gauges on/off showed negligible effect on the leak rate or the pressures for our measurements.

⁶Verified in the rate-of-rise test.

⁷The lowest leak rate which can be produced by the used dosing valve is 10^{-7} mbar l/s.

The above described effects on measurement can have two causes, the pumping of helium by the vacuum gauges itself and the contamination of the vacuum gauges due to longer periods of operation at higher pressures. The inverted magnetron type of gauges (in our case Pfeiffer PKR251) can pump gas, typical pumping speeds can be found in [Jou08] where the pumping speed for helium of 0.03 l/s is given. In the course of the conductance measurements, the vacuum gauges were operated continuously in the pressure range of 10^{-4} to 10^{-2} mbar from ~ 5 up to ~ 70 hours. That probably caused the contamination, which can result in a deviation of the measured pressures where the indicated pressure in the range $< 10^{-3}$ mbar is too low. Both of these effects would have a larger influence on the measurements made at lower leak rates (lower pressure).

Due to the fact that the pressure corrections and the effects of the vacuum gauges on the leak rate influence more lower leak rate values, uncertainties in the corresponding conductance's will be larger than indicated by the error-bars. In regard to this, the conductance obtained for the helium leak rates of lower than 10^{-6} mbar l/s can be excluded from assessing the valve conductance due to significant uncertainties. The remaining data gives 1.44×10^{-3} l/s and 4.37×10^{-3} l/s for the minimum and maximum value of the cryogenic vacuum conductance respectively.

3.7. Conclusion

The cryogenic vacuum valve was constructed in order to improve the vacuum at the trap chamber in the ALPHATRAP experiment. The valve operates by reducing an opening through which a rest-gas flows to the chamber. Therefore, the conductance of the valve in closed position was measured. Due to problems in the measurement process discussed in the section above the conductance could not be accurately measured. It is estimated to be between 1.44×10^{-3} - 4.37×10^{-3} l/s. The corresponding conductance at 4 K temperature is found from Equation 3.27. Comparing this values to the conductance of the tube segment $C_t = 0.178$ l/s (He, 4 K) (see section 3.3) results in a pressure reduction factor of about 170 - 530 that can be expected from the valve for helium gas at 4 K temperature. However, calculation of trap chamber pressure did not consider a cryopumping effect on the surface of the tube segment itself. Before a steady state gas flow is established, a rest-gas mono-layer will be formed on the tube walls. The mono-layer formation time will be longer if the valve is closed. This effect could significantly contribute to the storage time of the ions even if the conductance of the valve is high.

4. Cryogenic piezoelectric switch

4.1. Operating environment and requirements

As it was mentioned in section 2.4, the switch must operate in the ALPHATRAP ion detection system environment. Therefore, the operating conditions for the switch are 4 K temperature, ultra-high vacuum and strong magnetic field. There are several reasons why it would be an advantage to use an electromechanical switch for switching of the components in the ALPHATRAP electronics system. Two main applications where the the switch could be used are

- Switching of the RF excitation lines connected to the trap electrodes
- High quality factor (Q) resonator switching

Due to imperfect shielding properties of the RF excitation lines a radio frequency noise can reach the trap electrodes where it will interfere with the measurement process. Hence, it would be desirable to switch off these lines when they are not used in the measurements. When a switch is used for disconnecting the excitation lines, the voltage appearing on the trap electrodes u scales as [Stu13]

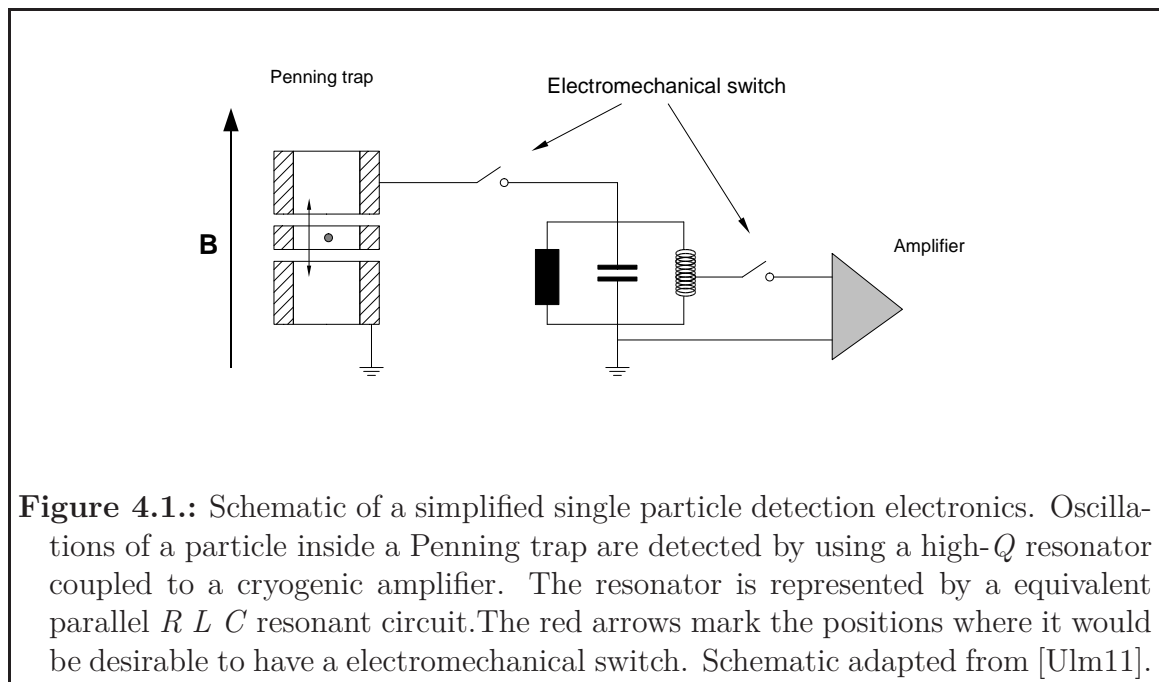
$$u \sim r_{\text{on}} u_0, \tag{4.1}$$

where r_{on} is the resistance in on state of a switch and u_0 is the voltage on the trap electrodes when the excitation lines are open. Solid state switches, which are typically used in this application, have an r_{on} resistance of $\sim 2 \Omega$, where it has to be additionally considered that leakage currents are present in the off position in these switches. Using an electromechanical switch instead could have twofold benefit. If the r_{on} resistance of the electromechanical switch is lower than $\sim 2 \Omega$, the excitation lines would be effectively disconnected with a lower voltage u on the trap electrodes. While in the off position, the electromechanical switch would have insignificant leakage currents since electrical contact is realized mechanically. This would result in a efficient isolation from the excitation lines than in the current situation by using solid-state switches.

Switching off a high- Q resonator is needed when techniques to cool down a trapped particle below 4 K temperature are used (e.g. laser cooling). In that case, the particle must be effectively decoupled from the “heat bath” of the resonator at 4 K. The main intention of such a switch is to provide an effective decoupling of the

particle and the resonator while preserving the Q as much as possible. High Q value of the resonator ensures good signal-to-noise ratio and gives a shorter cooling times for the trapped particles. The solid-state switches, which are also used here, have a significant shortcomings considering the influence on the Q value. The resonator RF electric field transmitted through the wire dissipates energy by inducing dielectric losses in the switch itself (a semiconductor material) and the housing material of the switch. It is therefore important to minimize the dielectric losses to preserve the Q value. Advantage of using an electromechanical over a solid-state switch is that the switch contact terminals can be separated from the actuating mechanism, which can be a source of the losses. The location of the switch for this application is shown in Figure 4.1.

The problem in constructing an electromechanical switch is how to actuate the switch considering our extreme environment, the limited space available and provided that the operating voltage is low as possible. Therefore, it was decided to use a piezoelectric bender plate as an actuator, since piezoelectric elements are suitable for operation in our environment, take up little space and require relatively low operating voltages. In order to preserve a high- Q the switch was constructed in a specific way, where the contact terminals are moved away and shielded from the actuator (piezoelectric bender plate). This ensures that the dielectric losses coming from the material of the bender plate are minimized.



4.2. Piezoelectric bender plates

The tests in this chapter are performed with the PL140.11 piezoelectric bender plate produced by the Physik Instrumente GmbH & Co.. The PL140.11 model has a nominal displacement of ± 1 mm at room temperature, which is achieved under operating voltage of 60 V. Figure 4.2 shows the operation principle of the PL140.11 model.

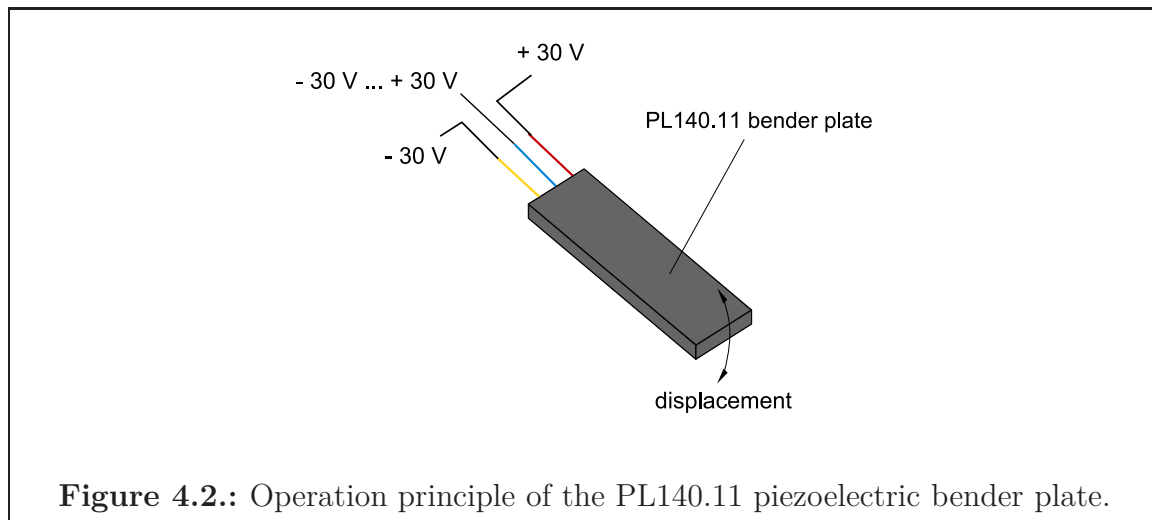


Figure 4.2.: Operation principle of the PL140.11 piezoelectric bender plate.

In all tests described in this chapter, displacement of the bender plate is controlled by applying DC voltages as shown in Figure 4.2. On the outer red and yellow electrodes the voltages are fixed at +30 and -30 V. The voltage on the blue electrode (actuating voltage) can be adjusted from 0 to ± 30 V. The maximum actuating voltage in this chapter refers to + 30 or - 30 V on the blue electrode. By applying 0 V on the blue electrode the bender plate is not polarized and the displacement is zero, while applying +30 or -30 V gives the maximum displacement of 1 mm. For voltages in between 0 and +30 V on the blue electrode, the displacement is roughly proportional to the voltage. When using the bender plate as an actuator in a switch, two factors are important for a reliable switching in our application, the maximum displacement and the contact force (at the voltages specified above). A sufficiently large displacement is needed to produce (ideally) infinite electrical resistance when the switch is in the off state, and a sufficiently large contact force is needed to obtain a low electrical resistance when the switch is in the on state (r_{on}). Therefore, if displacement at 4 K temperature reduces to $\sim 10 - 15$ % of its nominal value [VM00] but the contact force remains adequate to produce low contact resistance, it could still be possible to use the bender plate as an actuator in our environment.

4.3. Displacement and contact resistance

As discussed in the previous section, the nominal displacement of the PL140.10 piezoelectric bender plate at room temperature is ± 1 mm. When operated in an unipolar way, displacement at liquid helium temperature is ~ 10 to 15 % of its nominal value. Another issue concerning the operation at cryogenic temperatures is the possible occurrence of a "bimetallic strip" effect. Depending on the thermal expansion properties of the materials from which the bender plate is made of, a cryogenic temperatures could produce bending even without applying an actuating voltage. If this effect is "strong", it could lead to problems in the switching. For a switch constructed to function as a simple unipolar switch, as in our case, where the contact terminals are either connected or disconnected from each other, this is of particular concern. Therefore, to assess whether the piezoelectric bender plate is suitable in our application, the displacement and the contact resistance were tested before the switch design was considered in more detail.

4.3.1. Displacement at cryogenic temperatures

The displacement test were performed with the first version of the switch shown in Figure 4.3. The piezoelectric bender plate is mounted on an aluminum holder, where one side is fixed to the holder and the free side has a contact terminal. The fixed side is insulated from the aluminum holder by a Kapton foil. One contact terminal is a tile of copper, attached with screws and clamping 2-3 mm in free length on the top of the bender plate. A second contact terminal is the M1.6 screw made of brass, by which the distance to the contact terminal on the bender plate can be adjusted. By rotating the screw for one complete turn the screw advances by $360 \mu\text{m}$. Therefore, a rotation of $1/8$ and $1/4$ turns gives $\sim 90 \mu\text{m}$ and $\sim 40 \mu\text{m}$ step sizes, which is possible to set by manually rotating the screw. To ensure that the screw retains the set position a spring is fitted between the head of the screw and the aluminum holder.

The screw rotations steps can be used to estimate the bender plate displacement also at cryogenic temperatures. The distance between the bender plate and the brass screw contact terminals set at room temperature will be affected by cooling down the switch. However, the length of the brass screw and the thickness of the aluminum holder are approximately the same, about 1 cm, while the integrated linear thermal contraction coefficient ($\Delta L/L$ (%)) from 293 K to 4 K is 0.414 for aluminum and 0.384 for brass [VR10]. Therefore, the difference in the linear contraction upon cool-down from room to 4 K temperature between the aluminum holder and the brass screw will be $\sim 3 \mu\text{m}$. This is insignificant compared to the $\sim 40 \mu\text{m}$ step size used to adjust the contact terminals distance. Due to the above, in a displacement and contact resistance tests, it is assumed that the distance between the contacts set at room temperature is the same at 4 K temperature.

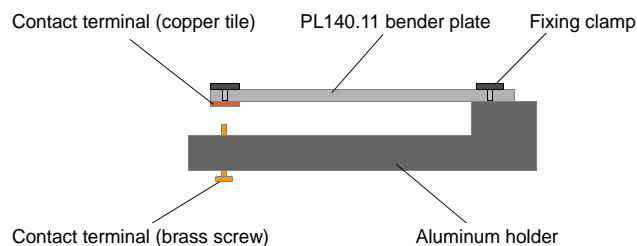


Figure 4.3.: Schematic drawing of the first version of the switch. Shown setup was used to test the displacement and the contact resistance at cryogenic temperatures. In measuring contact resistance by a four-wire sensing method, the wires were soldered to the contact terminals indicated on the drawing. A photograph of the above switch is given in Figure A.2

A displacement test at 77 K temperature was performed in an open liquid nitrogen cryostat (Styrofoam), where it was found to be about $350\ \mu\text{m}$. A displacement test at 4.2 K temperature was performed by submerging the switch in a liquid helium dewar where the switch was attached to a G10 rod. By setting the distance between the contact terminals approximately 40 to $90\ \mu\text{m}$ ($1/8$ and $1/4$ turns on the screw), electrical contact was realized. The DC contact resistance was measured using a Fluke 179 multimeter. For maximum actuating voltage of 30 V (see section 4.2) the contact resistance of 1 to $2\ \Omega$ was measured, while setting the actuating voltage to zero resulted in an infinite contact resistance on the multimeter. For the distance between the contact terminals approximately above the $130\ \mu\text{m}$ it was no longer possible to realize the electrical contact.

When cooling down the switch a sporadic electrical contact was observed, however this could rather be attributed to mechanical vibrations than bending of the piezoelectric bender plate itself. Unstable environment caused by the instant cooling process, producing boiling of the cryogenic liquid, is likely to be the reason for the contacting during the cool-down. When the switch is thermalized to the cryogenic environment the sporadic contacting stops. The contact resistance measured in the displacement test above is used only as an indication of the contact and can not be taken as a reliable information. The wires soldered on the contact terminals of the switch, about 4 m in length and 0.5 mm in diameter, were connected by crocodile clips to the multimeter. This can easily lead to overestimated values. A more precise method for measuring the contact resistance of the switch at 4 K temperature is described in the following section.

4.3.2. Contact resistance at 4 K temperature

Under assumption that the contact force produced by the piezoelectric bender is the same at room and 4 K temperature the contact resistance at 4 K must be lower, since the electrical resistance of switch contact terminals (copper and brass) reduces from room to 4 K temperature [VR10]. However, the nominal blocking force of the piezoelectric bender plate also reduces with the lower temperatures. The resulting effect of these two factors on the contact resistance is difficult to predict without a precise measurement.

In order to determine the contact resistance with a better precision than in the LHe displacement test, discussed in the section above, a four-wire sensing method was performed. The method uses two separate pairs of wires as shown in Figure 4.4. One pair of wires is used for “pushing” a constant I current through the test object, and the other pair of wires is used for sensing the corresponding voltage drop U over the test object. Since the input resistance of the multimeter measuring the voltage drop is high (typically in the $M\Omega$ range), it is assumed that no current is flowing through the R_{w2} and R_{w3} of the voltage sensing wires. In that case, the resistance of the test object is given as

$$R_{object} = U/I. \quad (4.2)$$

Hence, by setting the the current I and measuring the corresponding voltage drop U , the resistance of the test object can be measured eliminating the resistance R_{wx} from the wires in both the current and voltage sensing leads.

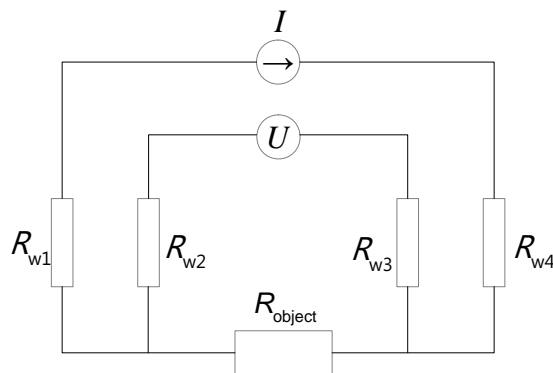


Figure 4.4.: Four-wire sensing method scheme: I constant current source, R_{wx} resistance of the wires connected to the test object, U voltage drop measured on the test object excluding the voltage drops of the wires.

By using the four-wire sensing, the switch (Figure 4.3) DC contact resistance was measured to be about 150 m Ω at room temperature. The same switch was used in the four-wire resistance measurement at 4 K temperature.

The test at cryogenic temperature was performed in a setup, where the switch was cooled to ~ 3 K by using a pulse tube cryocooler (Sumitomo SRP-062B-F-50H), as shown in Figure 4.5. The cryocooler uses a cyclic process of expanding and compressing a helium gas to produce cryogenic temperatures, which are attained in two stages. The second stage where test objects are located reaches ~ 3 K.

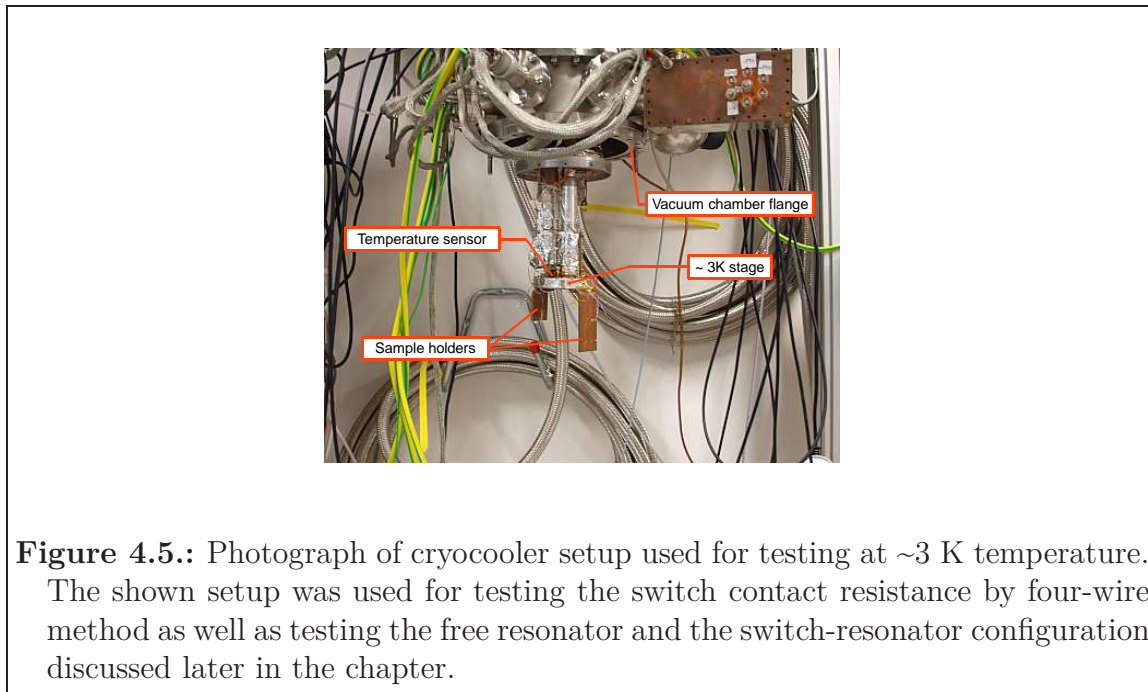


Figure 4.5.: Photograph of cryocooler setup used for testing at ~ 3 K temperature. The shown setup was used for testing the switch contact resistance by four-wire method as well as testing the free resonator and the switch-resonator configuration discussed later in the chapter.

The switch was attached to the copper sample holder by using screws, while a thermal thermal conducting grease was applied on the contact surfaces in order to ensure good thermalization. The sample holder is covered by an aluminum shield (not shown), which provides the shielding from the external thermal radiation coming from the surfaces at room temperature. A larger steel vacuum chamber is attached by using the CF flange, shown on the top. In operation, the vacuum chamber is first pumped down to 10^{-4} mbar in order to reach the isolating vacuum, and then the cryocooler starts the cool-down process.

In the first attempts to determine the contact resistance of the switch in the cryocooler setup, the four wires were connected to the Fluke 8846A multimeter that has a four-wire resistance measurement function. The multimeter automatically excludes the resistance of the wires, however, it was not possible to get an unambiguous readout from the multimeter. The measured contact resistance was in the $m\Omega$ range, but exchanging the poles of the current carrying wires resulted in two different values for the contact resistance. Even the exchange of the current and the voltage sensing wire pairs resulted in a varying value for the contact resistance. At the end different results in the range from 1 to 40 $m\Omega$ were obtained for the contact resistance. Since these wire pairs are soldered to the same contact points it was not immediately clear what causes different values. In order to describe the above

problem in a more complete way the four-wire method scheme shown above must include a large temperature gradient of the cryocooler setup, shown in Figure 4.6.

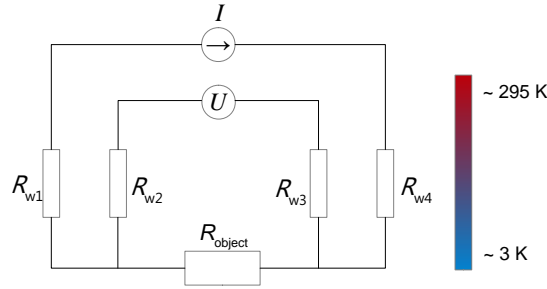


Figure 4.6.: Four-wire sensing method scheme corresponding to measurement in the cryocooler setup. The wires connected to the test object are found in a large temperature gradient. This can produce a thermocurrent that interferes with the contact resistance measurement.

If the current or the voltage sensing wires are made of different material, the temperature gradient could produce a thermocouple in the leads. The principle of the thermocouple is based on the Seebeck effect, in which two different conductors connected in a loop produce a current flow when their junctions are at different temperatures. The current depends on the Seebeck coefficients of the conductors and the temperature difference. This effect could produce a current in addition to the current sent from the multimeter. Depending on the materials involved, the thermocurrent is added to or subtracted from the multimeter current

$$R_{object} = \frac{U}{I \pm I_{thermo}}. \quad (4.3)$$

Furthermore, a current can also flow through the multimeter. Even if this current is low, it can produce a large voltage drop since the multimeter resistance is high. These effects can result in a significant error when determining R_{object} . Effective way to circumvent these problems is to perform the four-wire method directly, this is described in the following.

The current wires were connected to the Hameg HMP4040 which provided a constant current, while the voltage drop on the contact point was measured by the Fluke 8846A. Setting a different current on the current source and measuring the corresponding voltage drops over the switch contact point allows to obtain the resistance of the contact by avoiding the above described errors. The measured current and voltage data obtained for the switch is shown in Figure 4.7.

The resistance of the contact is found from the line fit to the data points, where the slope of the line gives the contact resistance of 11 m Ω . It is important to note that this resistance is measured between the end point of the brass screw and the edge

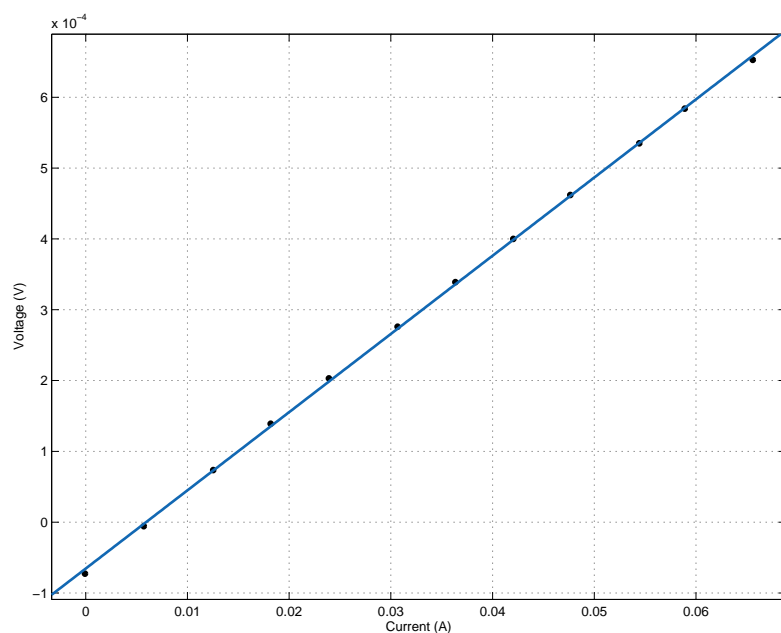


Figure 4.7.: Measured voltage and current from the four-wire measurement for the switch shown in Figure 4.3 at ~ 3 K temperature. The linear fit gives the resistance of $11 \text{ m}\Omega$. When the current is set to zero, the voltage drop measured on the multimeter is not zero, this indicates there is an additional current flowing in the wiring.

of the tile contact terminals on the bender plate, as shown in Figure 4.3. Therefore, the actual contact resistance is lower than $11 \text{ m}\Omega$.

4.4. Design of the piezoelectric cryogenic switch

Considering that the tests described in the previous section showed assuring results on the displacement and contact resistance, a switch version for the testing in combination with a high- Q resonator was constructed. The switch used for the tests in the section section 4.3 could in principle be used here. However, that design is not suitable if preserving a high- Q is a requirement. The construction considering the arguments described in section 4.1 is shown schematically in Figure 4.8. The bender plate is mounted in an metal housing which provides the shielding of the contact point, while a ceramic rod (a low loss dielectric) is used for moving the contact point away from the piezoelectric bender plate. The screw (ground contact terminal) is placed in a holder at the bottom, which enables the adjustments of the distance

between the contact terminals.

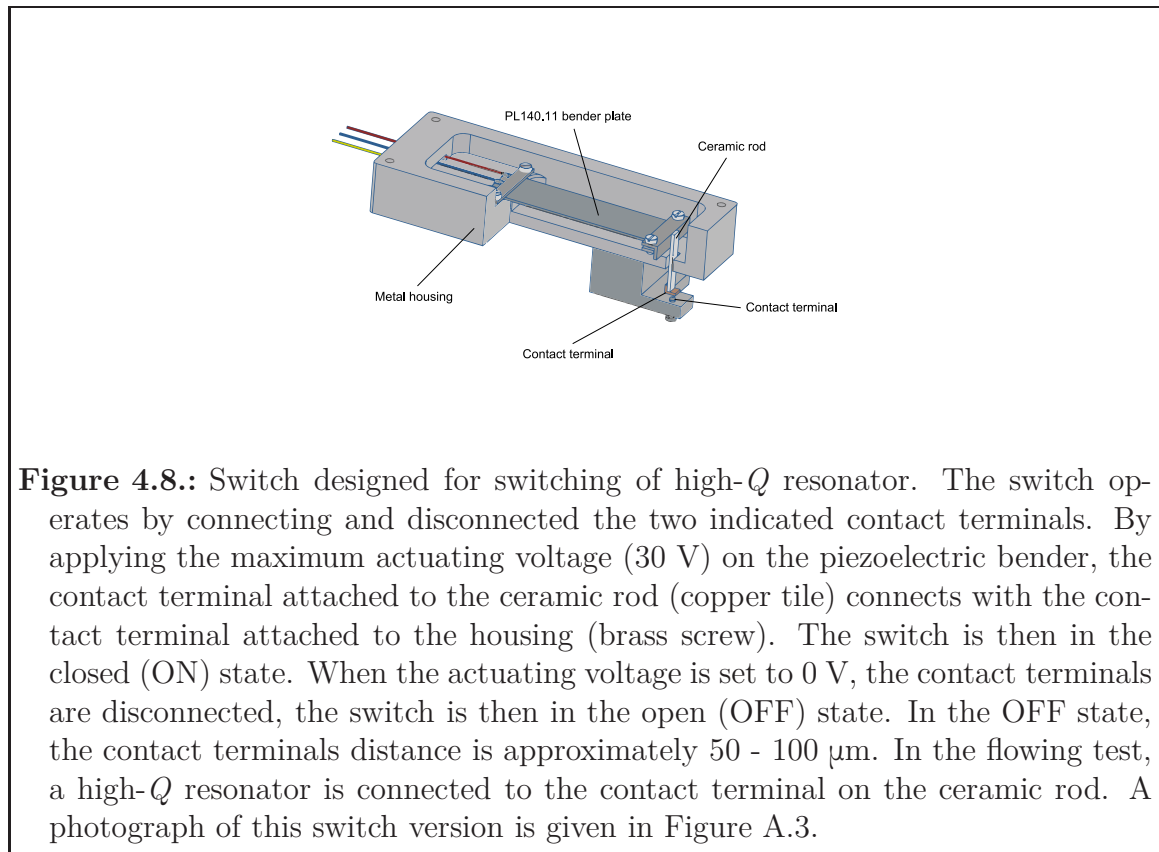


Figure 4.8.: Switch designed for switching of high- Q resonator. The switch operates by connecting and disconnected the two indicated contact terminals. By applying the maximum actuating voltage (30 V) on the piezoelectric bender, the contact terminal attached to the ceramic rod (copper tile) connects with the contact terminal attached to the housing (brass screw). The switch is then in the closed (ON) state. When the actuating voltage is set to 0 V, the contact terminals are disconnected, the switch is then in the open (OFF) state. In the OFF state, the contact terminals distance is approximately 50 - 100 μm . In the flowing test, a high- Q resonator is connected to the contact terminal on the ceramic rod. A photograph of this switch version is given in Figure A.3.

The piezoelectric bender plate is enclosed in an aluminum housing. It is fixed on one end by a clamp and isolated by using a Kapton foil. A metal clip is attached on the free side of the bender plate, taking about 2 to 3 mm of the bender plate tip. A ceramic rod (Al_2O_3) is bonded to the metal clip by using a Stycast FT 2850 epoxy glue. The contact terminal (copper tile) on the ceramic rod is also bonded by the same epoxy glue. The the ground contact terminal is a brass screw attached to the aluminum holder at the bottom of the aluminum housing. Figure A.3 shows a photograph of the piezoelectric switch described above. The switch used in the test with a high- Q resonator discussed in the next chapter.

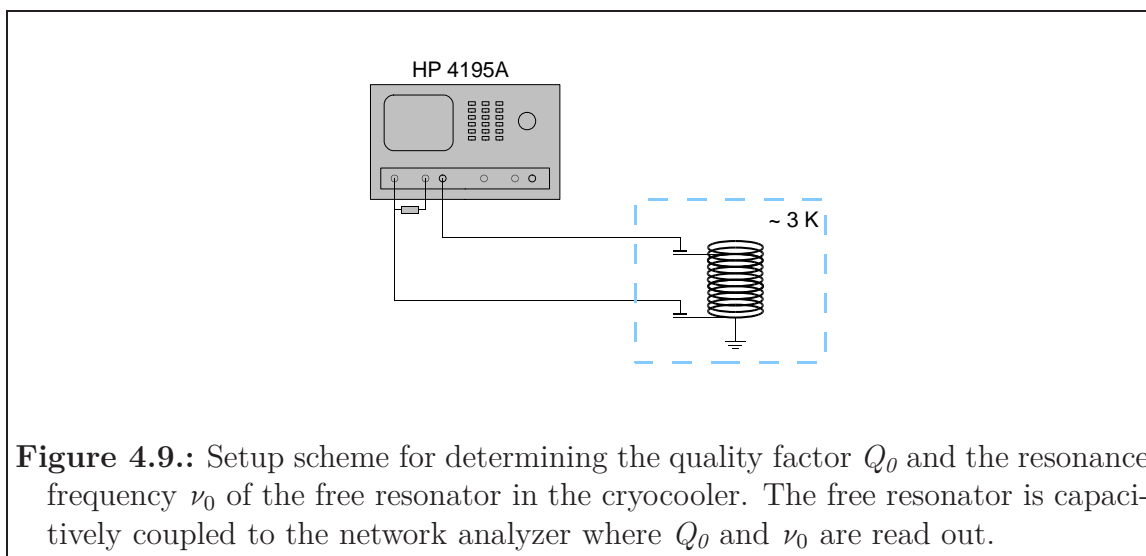
4.5. Switching a high quality factor resonator using a piezoelectric switch

This chapter describes the tests were the piezoelectric switch, presented in the section above, is used to switch on/off a high- Q resonator. The resonator was first tested individually, in order to find the resonance frequency and the Q value of the free resonator. Thereafter, in the same setup, the switch is connected to the

resonator. Measuring the Q values and the resonance frequencies of the these two configurations allows to determine the effects of the switch on the resonator.

4.5.1. Characteristic of the high quality factor resonator

The resonator used in the following has a coil made of Niobium-titanium (NbTi) superconducting wire wound in a toroidal geometry, which has a critical temperature of ~ 9.5 K. The wire is wound on a coil body made of PTFE¹ (a low dielectric loss material) and enclosed in the housing made of oxygen-free high thermal conductivity copper. Before testing of the switch-resonator configuration, the quality factor and the resonance frequency of the free resonator was found in the cryocooler setup (Figure 4.5). Figure 4.9 shows the setup scheme for that measurements, where resonator is capacitively coupled via coaxial lines to the HP 4195A network analyzer operating in T/R (Transmit/Receive) mode. Upon cool-down to ~ 3 K temperature, the quality factor and the resonance frequency can be read out directly from the resonance curve on the network analyzer.

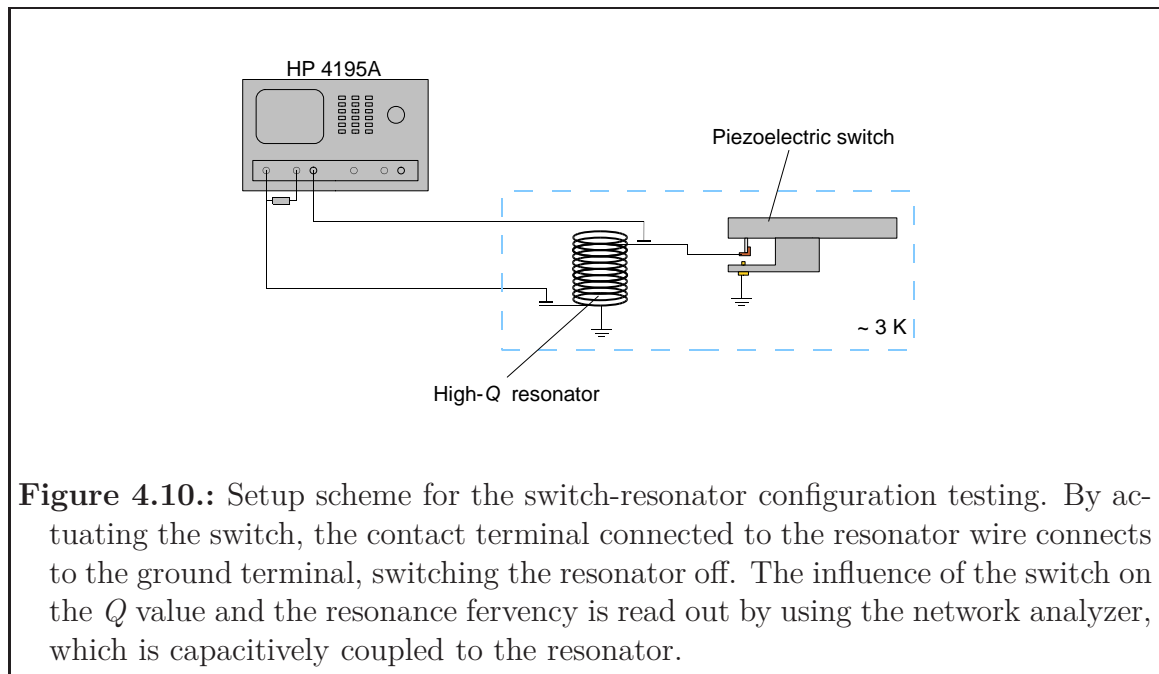


From the above described measurement a quality factor of $Q_0 = 65000$ at resonance frequency of $\nu_0 = 836.0$ kHz was determined for the free resonator. Having found these values allows to assess the effects of connecting an additional component to the resonator.

¹Polytetrafluoroethylene, which is commonly referred to as Teflon.

4.5.2. Test setup and procedure for the switch-resonator configuration

The switch-resonator configuration the was tested in the same cryocooler setup as the resonator discussed above. Figure 4.10 shows the measurement scheme of the switch-resonator configuration. The difference to the free resonator scheme is that the end of the resonator terminal wire, capacitively coupled to the receive port of the network analyzer, is now connected the switch. The connecting wire (Omega Engineering IEC-TFCP-005-15M, ~ 20 cm in length) is soldered to the contact terminal on the switch and the resonator terminal wire. The resonator and the switch where fixed under a 3 K stage plate of by using screws, where a thermal conducting grease was applied on the contacting surfaces to ensure a good thermal contact. A photograph of the switch-resonator configuration setup in the cryocooler is shown in the Figure A.4.



The tests of switch-resonator configuration were performed in a default state of the switch when no actuating voltage is applied on the piezoelectric bender plate. The switch contact terminals are disconnected and the actuating voltage must be applied to connect the two terminals. By applying the maximum actuating voltage (30 V) the resonator is connected to the ground terminal. Therefore, the resonance curve measured on the network analyzer should completely disappear. This indicates successful switching off of the resonator. By setting the actuating voltage to 0 V the resonance curve should reappear. Whereby, the main objective is that the quality factor and the resonance frequency stay as close as possible the Q value measured for the free resonator.

4.5.3. Measurement results

Figure 4.11 shows measurement results obtained for the switch-resonator setup configuration described in the previous section. When the switch is in the off state the contact terminals are disconnect and resonator shows a resonance curve, indicated in blue. By applying the maximum actuating voltage, the switch is in the on state and the contact terminals are connected. The resonator terminal is then connected to the ground, which is indicated in red. In this way, the resonator can be switched between the two states indicated in blue and red. Additionally, The quality factor of $Q_{sr} = 56000$ was determined at the resonance frequency of $\nu_{sr} \sim 806.3$ Hz for this configuration. A small shifts from the resonance frequency on the order ~ 10 Hz were observed when the resonator was switched between the two states.

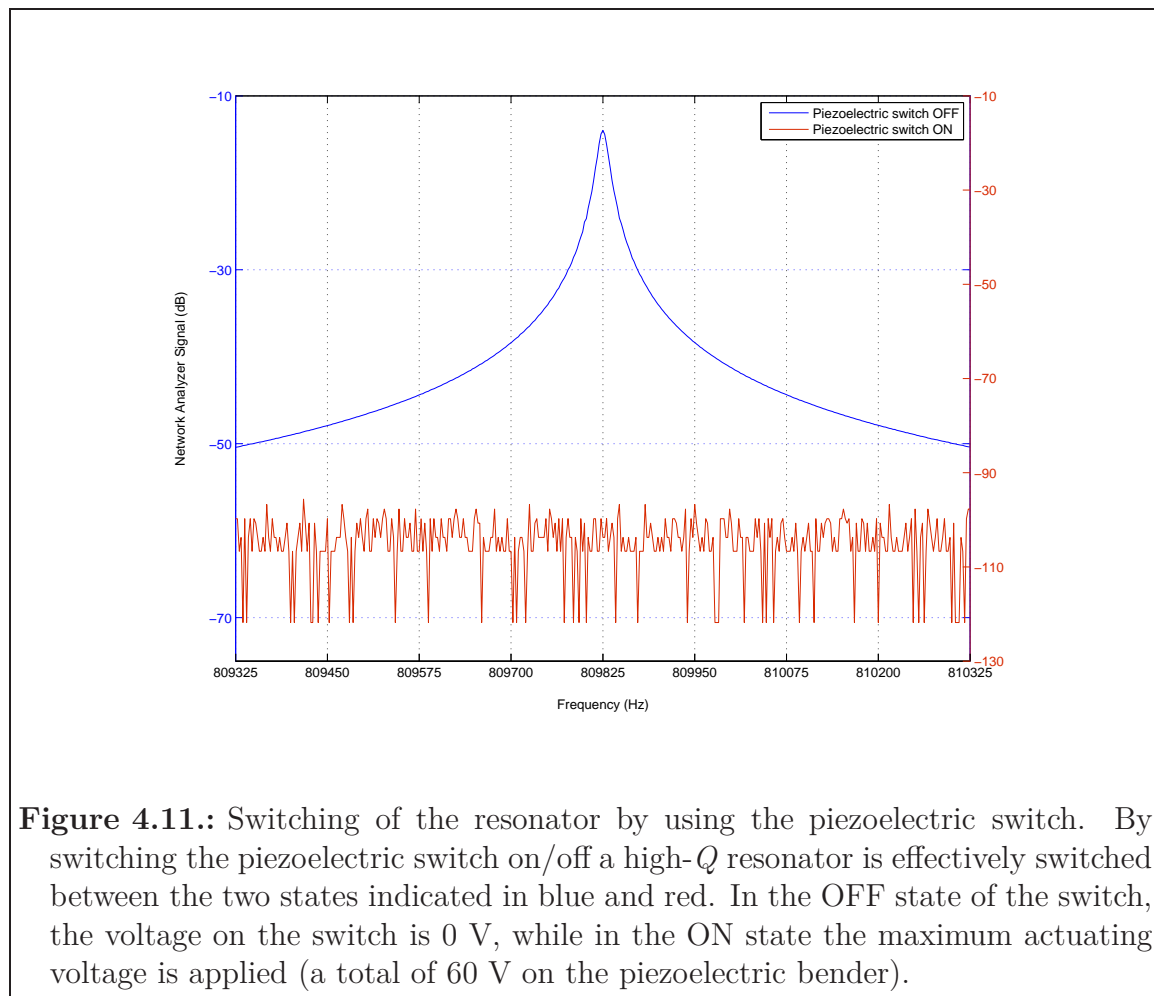


Figure 4.11.: Switching of the resonator by using the piezoelectric switch. By switching the piezoelectric switch on/off a high- Q resonator is effectively switched between the two states indicated in blue and red. In the OFF state of the switch, the voltage on the switch is 0 V, while in the ON state the maximum actuating voltage is applied (a total of 60 V on the piezoelectric bender).

From comparing the quality factors (Q_0 , Q_{sr}) and the resonance frequencies (ν_0 , ν_{sr}) of free resonator and the switch-resonator configuration shows that introducing the switch resulted in a quality factor reduction ($\Delta Q/Q$) of ~ 15 %, while the change in the resonance frequency ($\nu_0 - \nu_{sr}$) was ~ 30 Hz. This test showed that by using the

piezoelectric switch a high- Q resonator can be effectively switched off, while having a relatively little influence on the quality factor.

In a separate test, performed at room temperature, the capacitance of the switch was found to be 1.3 pF (± 0.1 pF max. error). This was measured with an Agilent E4980A L C R meter at 1 kHz when the distance between the contact terminals is set to ~ 50 μm .

4.6. Conclusion

Cryogenic piezoelectric switch was constructed in order test alternatives to the solid-state switches currently used in the cryogenic electronic. The aim was to have an improvement over undesirable properties of solid-state devices (e.g. leakage currents and dielectric losses) and to achieve a lower resistance when the switch is in the on state than typically found in solid-state switches (~ 2 Ω). For the piezoelectric switch constructed within this thesis the following properties were found

- Switch resistance in the on state $r_{\text{on}} \sim 10$ m Ω
- Insignificant leakage currents
- Capacitance of ~ 1 pF (at 1 kHz, ~ 50 μm contact distance)
- Relatively small dielectric losses

Furthermore, it was shown that the switch can be used to switch on/off a high- Q resonator, with a relative small influence on the Q value ($\Delta Q/Q \sim 15$ %) and effects on the resonance frequency ($\Delta\nu \sim 30$ Hz). Therefore, considering these promising results, the switch can be used to improve the capabilities of ion detection electronic or in a cryogenic applications when better performing alternatives to the solid-state switches are needed. Additionally, except from the actuating piezoelectric element, the construction of the switch is not based on special production process and does not involve costly materials.

Bibliography

- [Ber65] AS Berman. Free molecule transmission probabilities. *Journal of Applied Physics*, 36(10): 3356–3356, 1965.
- [CC05] Austin Chambers and A Chambers. *Modern vacuum physics*. Chapman & Hall/CRC Boca Raton, 2005.
- [Her99] Nikolaus Helmut Hermanspahn. *Das magnetische Moment des gebundenen Elektrons in wasserstoffartigem Kohlenstoff (C 5+)*. PhD thesis, Johannes Gutenberg Universität Mainz, 1999.
- [Jou08] Karl Jousten. *Handbook of vacuum technology*. John Wiley & Sons, 2008.
- [LUH14] José R Crespo López-Urrutia and Zoltán Harman. Emission and laser spectroscopy of trapped highly charged ions in electron beam ion traps. In *Fundamental Physics in Particle Traps*, pages 315–373. Springer, 2014.
- [Man86] R Mann. Total one-electron capture cross sections for ar q+ and i q+ ions in slow collisions on h2 and he. *Zeitschrift für Physik D Atoms, Molecules and Clusters*, 3(1): 85–90, 1986.
- [O’H05] John F O’Hanlon. *A user’s guide to vacuum technology*. John Wiley & Sons, 2005.
- [RI67] A Roth and A Inbar. The force cycle of vacuum gasket seals. *Vacuum*, 17(1): 5–13, 1967.
- [Rot12] Alexander Roth. *Vacuum technology*. Elsevier, 2012.
- [Stu11] Sven Sturm. *The g-factor of the electron bound in 28 Si 13: The most stringent test of bound-state quantum*. PhD thesis, Johannes-Gutenberg Universität, Mainz, 2011.
- [Stu13] Sven Sturm. private communication, 2013.
- [SWB13] Sven Sturm, Günter Werth, and Klaus Blaum. Electron g-factor determinations in penning traps. *Annalen der Physik*, 525(8-9): 620–635, 2013.
- [Ulm11] Stefan Ulmer. *First observation of spin flips with a single proton stored in a cryogenic Penning trap*. PhD thesis, Ruprecht-Karls Universität, Heidelberg, 2011.
- [VM00] R Vaccarone and F Möller. Cryogenic behavior of piezoelectric bimorph actuators. In *Advances in Cryogenic Engineering Materials*, pages 275–282. Springer, 2000.

- [VR10] Guglielmo Ventura and Lara Risegari. *The art of cryogenics: low-temperature experimental techniques*. Elsevier, 2010.

A. Appendix

A.1. Gas flow relations

Transmission probability coefficient for a rectangular thin slit [Ber65, O'H05]

For the slit height $h \ll$ width b and any length l . Transmission probability coefficient is given by $a = k_1 - k_2$, where k_1 and k_2 are found from the following equations ($L = l/h$)

$$k_1 = \frac{1}{2} \left(1 + \left(1 + L^2 \right)^{\frac{1}{2}} - L \right) \quad (\text{A.1})$$

$$k_2 = \frac{\frac{3}{2} \left(L - \ln \left[L + \left(L^2 + 1 \right)^{1/2} \right] \right)^2}{L^3 + 3L^2 - 4 - \left(L^2 + 4 \right) \left(L^2 + 1 \right)^{1/2}}. \quad (\text{A.2})$$

Waviness in a Sealing process

The function describing the waviness of the surfaces in the sealing process found in [RI67] is given by

$$F((a/2)/A) = \frac{2 \left(1 + 2 \frac{a/2}{A} \right)^2 \left(1 + \frac{a/2}{A} \right) \left(1 + \frac{1}{\cos(\alpha)} \right)}{\left(1 + \frac{1}{\cos(\alpha)} \right) \left(1 + \frac{a/2}{A} \right) \left(1 + 2 \frac{a/2}{A} \right)^{1/2} \left(\pi - \arctan \left[\frac{-1}{\left(1 + 2 \frac{a/2}{A} \right)^{1/2}} \right] \right) + 1 + 2 \frac{a/2}{A}}. \quad (\text{A.3})$$

A.2. Photographs



Figure A.1.: Cryogenic vacuum valve, shown in a assembly that was used to leak test the valve in the vacuum mode. The holes seen at the bottom of the valve body are used to vent the gases form screw threads of the indium seal.

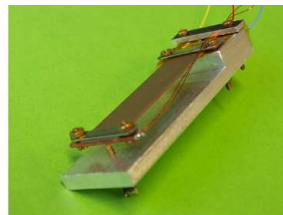
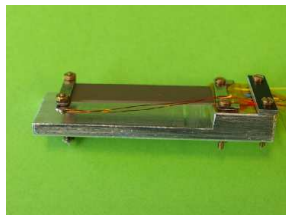
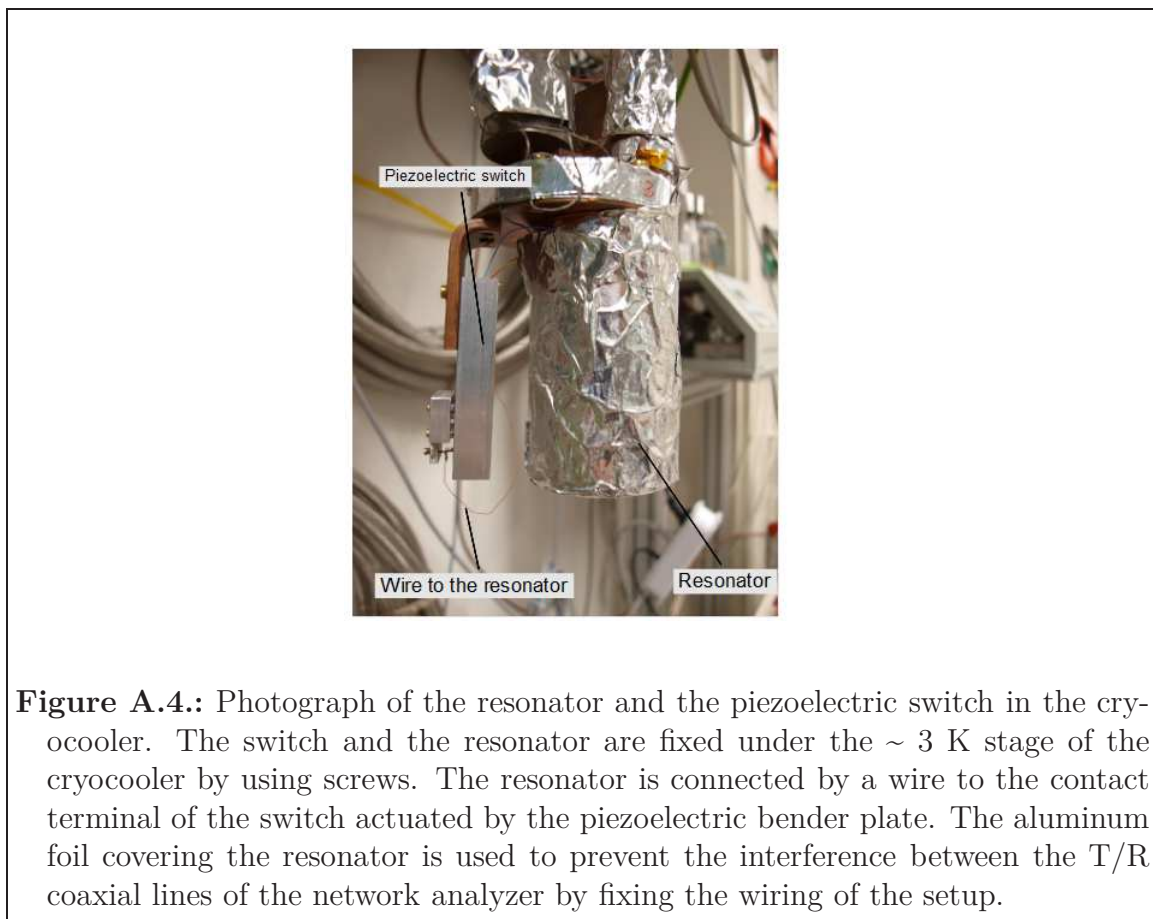
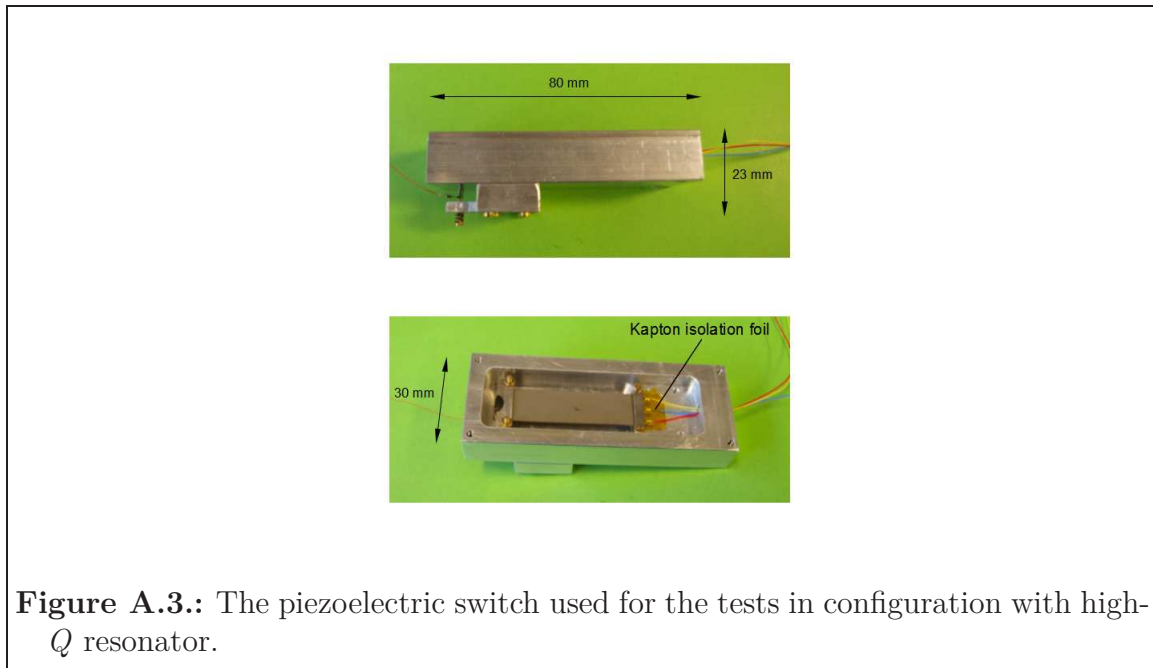


Figure A.2.: First version of the cryogenic switch that was used for testing the displacement at liquid-nitrogen and liquid-helium temperatures and measuring the contact resistance at ~ 3 K in the cryocooler.



Acknowledgments

I would like to thank to Prof.Dr. Klaus Blaum for supervision of my project, giving me the opportunity at to be a part of the MPI-K and creating a good atmosphere in the group.

I would like to thank to Dr. Sven Sturm for the supervision my work, his time and patience in discussions about physics and many practical advices that make life in experimental physics easier.

Thanks to the following people with whom I often had discussions or got advice on technical issues: Andreas Weigel - electronics related discussions and the idea with the spring on the switch. Christian Roux - correcting the text, advices for the presentations and ... correcting the text. Tommi Eronen - for my vacuum stuff related "?". Sergey Eliseev - storage-times and vacuum-cryo discussions. Mikhail Goncharov - some, but important LabView hints.

Thanks to the people from MPI-K Engineering Design Office and Precision Mechanics Shop with a special thanks to the people from the Apprentices' shop.

Furthermore, I would like to thank the rest of the people from PENTATRAP, PIPERADE and THE-TRAP for friendly and pleasant working environment.

Erklärung:

Ich versichere, dass ich diese Arbeit selbstständig verfasst habe und keine anderen als die angegebenen Quellen und Hilfsmittel benutzt habe.

Heidelberg, den (Datum)

